Physica D 393 (2019) 54–67

Contents lists available at ScienceDirect

Physica D

journal homepage: www.elsevier.com/locate/physd

Asymmetry in crystal facet dynamics of homoepitaxy by a continuum model

Jian-Guo Liu [a], Jianfeng Lu [a,b], Dionisios Margetis [c,*], Jeremy L. Marzuola [d]

[a] Department of Mathematics and Department of Physics, Duke University, Durham, NC 27708, United States
[b] Department of Chemistry, Duke University, Durham, NC 27708, United States
[c] Department of Mathematics, and Institute for Physical Science and Technology, and Center for Scientific Computation and Mathematical Modeling, University of Maryland, College Park, MD 20742, United States
[d] Department of Mathematics, University of North Carolina, Chapel Hill, NC, 27599, United States

HIGHLIGHTS

- We formulate a singular-diffusion PDE model from continuum limit of step flow.
- We construct an explicit solution of the PDE in absence of elasticity.
- We predict that top and bottom facets of periodic corrugations are asymmetric.
- We compare analytical results against numerical simulations.

ARTICLE INFO

Article history:
Received 1 May 2017
Received in revised form 18 October 2018
Accepted 22 January 2019
Available online 31 January 2019
Communicated by K. Promislow

Keywords:
Crystal surface
Epitaxial relaxation
Facet
Degenerate-parabolic PDE
Subgradient formalism
Burton–Cabrera–Frank (BCF) model

ABSTRACT

In the absence of external material deposition, crystal surfaces usually relax to become flat by decreasing their free energy. We study analytically an asymmetry in the relaxation of macroscopic plateaus, facets, of a periodic surface corrugation in 1+1 dimensions via a continuum model below the roughening transition temperature. The model invokes a continuum evolution law expressed by a highly degenerate parabolic partial differential equation (PDE) for surface diffusion, which is related to the nonlinear gradient flow of a convex, singular surface free energy with a certain exponential mobility in homoepitaxy. This evolution law is motivated both by an atomistic broken-bond model and a mesoscale model for crystal steps. By constructing an explicit solution to this PDE, we demonstrate the lack of symmetry in the evolution of top and bottom facets in periodic surface profiles. Our explicit, analytical solution is compared to numerical simulations of the continuum law via a regularized surface free energy.

1. Introduction

The epitaxial growth and relaxation of crystals include kinetic processes by which atoms are deposited from above, and are adsorbed and diffuse on a substrate to form solid films or other nanostructures. Hence, the crystal surface undergoes morphological changes [1–3]. If the crystal of the film matches that of the substrate, the processes pertain to homoepitaxy. Below the roughening transition temperature, macroscopic plateaus, called *facets*, may form. Their evolution is linked to various nanoscale phenomena [3]; for example, the stability of semiconductor quantum dots and the wetting/dewetting of crystal surfaces [4].

In this paper, we study implications of a continuum model based on a singular-diffusion partial differential equation (PDE) satisfied by the height profile in crystal surface relaxation, in the absence of external material deposition, in 1+1 dimensions. This evolution law encompasses continuum thermodynamics and mass conservation. The model is related to a nonlinear, weighted H^{-1}-gradient flow for a convex, singular surface free energy in homoepitaxy. The PDE is motivated by the continuum limit of the following models: (i) a *mesoscale* theory of line defects, steps, under diffusion-limited kinetics in monotone step trains [5,6]; and (ii) a family of *atomistic*, broken-bond models, in which the kinetic rates obey the Arrhenius law involving the energy barriers for atom hopping [7,8].

Physically, our continuum model reflects the presence of strong, isotropic *stiffness* of steps. This notion of step stiffness is related to the energy cost to create a step, and affects the local-equilibrium density, ϱ_s, of adsorbed atoms (adatoms). By the Gibbs–Thomson relation at equilibrium [9,10], this ϱ_s is an exponential function of the step chemical potential, μ_s, scaled by the Boltzmann energy, k_BT. The μ_s is defined as the change per atom in the step energy;

* Corresponding author.
E-mail addresses: jliu@math.duke.edu (J.-G. Liu), jianfeng@math.duke.edu (J. Lu), dio@math.umd.edu (D. Margetis), marzuola@math.unc.edu (J.L. Marzuola).

https://doi.org/10.1016/j.physd.2019.01.004
0167-2789/

and in principle expresses the joint effect of step stiffness and step–step interactions [2,11,12]. We assume that $|\mu_s|$ may be of the same order as or larger than k_BT; thus, the exponential dependence of ϱ_s on μ_s cannot be neglected. A similar chemical potential was used in [7] in the setting of adatom rates in order to derive continuum equations for the height profile from an atomistic perspective. At the continuum level, the assumption of an exponential law for ϱ_s versus μ_s implies that the adatom mass flux is proportional to the gradient of $\exp[\mu_s/(k_BT)]$, instead of the gradient of $\mu_s/(k_BT)$ as, e.g., in [13,14].

The continuum evolution law, henceforth called "exponential PDE", that results from the aforementioned exponential law expresses an asymmetry in the evolution of convex and concave parts of the surface. By assuming that step–step interactions are negligible, we show informally via construction of an analytical solution that an implication of the PDE is an *asymmetry* in facet evolution: top and bottom facets evolve differently in a periodic surface corrugation in 1+1 dimensions. In addition, we indicate numerically how such an asymmetry manifests in the presence of elastic-dipole step–step interactions. This more complicated case lies beyond the scope of our present study.

Our approach may offer a qualitative explanation of an asymmetry in the evolution of facets of one-dimensional, periodic surface corrugations observed via kinetic Monte Carlo simulations [15]. In this work [15], the (counter-intuitive) asymmetry in facet evolution is attributed to the relatively large amplitude of the initial height profile. Here, we view the asymmetry in facet dynamics as a direct consequence of the exponential PDE for the height. In this vein, we should also mention experimental observations of annealed gratings of Si with evolving facets [16]. These observations evade a complete understanding (see, e.g., [17]). Several pending questions emerge from our study. In particular, its extension to two spatial dimensions is the subject of future work.

It should be noted that in past continuum treatments of epitaxial growth, the exponential of $\mu_s/(k_BT)$ is typically linearized under the hypothesis that $|\mu_s| \ll k_BT$; see, e.g., [6,13,14,18–21]; see also the comment in [7]. This simplification in turn yields the standard (linear) Fick law for the mass flux in terms of the continuum-scale step chemical potential. The resulting continuum-scale evolution law does not distinguish between convex and concave parts of surface profiles.

We adopt an approach based on the following tools. (i) The extended-gradient (or, subgradient) formalism for the construction of an explicit solution to the PDE for the height profile across facets. This formalism is an extension of the PDE framework from the previous, familiar cases of evaporation-condensation and surface diffusion under linearization of ϱ_s versus μ_s, in which the metric space is L^2 or (non-weighted) H^{-1} [22,23], to the present, more complicated case of nonlinear gradient flow. (ii) Numerical simulations of the PDE by use of a regularized surface free energy, in the spirit of [18,24]. Our findings point to a few open questions about the connection of the microscale dynamics of crystals to the corresponding exponential PDE.

Our main results in this paper can be summarized as follows.

- We formulate a singular-diffusion PDE model. Away from facets, this model is consistent with the continuum limit of the Burton–Cabrera–Frank (BCF) theory for moving steps in 2+1 dimensions [5,6]. The PDE is also motivated by a family of KMC models of crystal surface relaxation that include both the solid-on-solid (SOS) and discrete Gaussian models [7,8].
- We consider the setting with a periodic surface corrugation in 1+1 dimensions, and treat facet edges as free boundaries. Accordingly, we informally develop an explicit solution for the height profile with recourse to the extended-gradient formalism in the absence of elasticity (i.e., without step–step interactions). Our construction invokes mass conservation and continuity of the continuum-scale step chemical potential across the facet. This procedure results in two coupled differential equations for the facet position and height, x_f and h_f. This approach forms an extension of the theory underlying [23,25–27] to the framework of the exponential PDE.
- In the context of the extended-gradient formalism outlined above, we show that the expansion of a facet is accompanied by a jump of the height profile at the facet edge; and the facet expands at finite speed.
- By heuristically analyzing the differential equation system for (x_f, h_f) in the periodic setting without elasticity, we predict that top and bottom facets are characterized by distinctly different evolutions. In particular, the top facet starts expanding regardless of its initial size; in contrast, the bottom facet expands if its initial size exceeds a certain critical length which we compute analytically.
- To test our analytical results, we compare them against numerical simulations by using a regularized surface free energy [18,24]. Our numerics confirm our prediction that top and bottom facets behave in distinct fashion.

From a physical perspective, the present, fully continuum treatment of facets, which are known to have a microscopic structure [2], leaves pending questions that need to be spelled out. The governing PDE can in principle be derived for monotone step trains. For the case with a linear-in-chemical-potential Fick law, see, e.g., [6,28]. This type of PDE, viewed as a continuum limit of step motion, may break down in the vicinity of facets, where the distance between steps changes rapidly [29–31]. Specifically, in the radial setting it has been shown that the continuum prediction based on the subgradient formalism may not be consistent with step flow; microscopic events of step annihilations on top of facets may significantly affect the surface slope outside the facet [31].

Hence, our results here are viewed as direct consequences of continuum thermodynamics and mass conservation. Our goal is to point out qualitative features of facet evolution that contrast some of the insights obtained previously by the continuum theory with a linearized law for the equilibrium adatom density versus step chemical potential. A striking feature predicted by our model is the asymmetry between top and bottom facets. The connection of our approach to step motion or KMC simulations in the presence of facets is left unresolved, and deserves further research in the near future.

1.1. Continuum framework

Next, we outline the main ingredients of the continuum model in canonical form. In Section 2, we provide details about the linkage of the continuum evolution laws to microscale models [6].

For a crystal surface evolving near a fixed crystallographic plane of symmetry, the surface free energy as a functional of height is convex and reads [32,33]

$$E[h] = \gamma \int_{\Omega} \left(|\nabla h| + \frac{g}{3} |\nabla h|^3 \right) \mathrm{d}x \qquad (\Omega \subset \mathbb{R}^2), \tag{1}$$

where γ is proportional to the energy cost to create a line defect (step), $h(x, t)$ is the graph of the surface, and the facet is identified with points (x, h) where $\nabla h(x, t) = 0$. It is important that, when $g = 0$, free energy (1) supports jumps in the height profile; see Section 4. Physically, $E[h]$ expresses the joint effect of step line tension ($|\nabla h|$ term), and elastic-dipole step–step repulsive interactions ($|\nabla h|^3$ term) where g is a non-negative constant equal to the relative strength of the interaction ($g \geq 0$) [32]; see also [11,12]. Formula (1) does not account for long-range elasticity of heteroepitaxy; see, e.g., [34,35].

Accordingly, the continuum-scale step chemical potential is defined as the variational derivative of $E[h]$, viz., [21]

$$\mu_s = \frac{\delta E}{\delta h} = -\gamma \operatorname{div}\left(\frac{\nabla h}{|\nabla h|} + g|\nabla h|\nabla h\right), \tag{2}$$

where we set the atomic volume equal to unity for algebraic convenience. Notice that (2) is ill-defined locally at the facet (where $\nabla h = 0$). By the Gibbs–Thomson relation [6,9,10], which is connected to the theory of molecular capillarity, the corresponding local-equilibrium density of adatoms is given by $\varrho_s = \varrho^0 \exp[\mu_s/(k_B T)]$, where ϱ^0 is a constant reference density. We note here that this relationship between the chemical potential and the density is a standard assumption, but not rigorously derived as of yet; see equation (20) in [36] and equations (7) and (13) in [37] for some discussion. For diffusion-limited kinetics, by which surface diffusion between steps is the rate-limiting process, by Fick's law the vector-valued adatom flux reads [6]

$$\mathbf{J} = -D_s \nabla \varrho_s = -D_s \varrho^0 \nabla e^{\mu_s/(k_B T)}, \tag{3}$$

where D_s is the surface diffusion constant.

The desired evolution PDE results by combining (2) and (3) with the familiar mass conservation statement

$$\partial_t h + \operatorname{div} \mathbf{J} = 0. \tag{4}$$

Consequently, the height profile, $h(x, t)$, obeys the PDE

$$\partial_t h = \Delta e^{-\beta \operatorname{div}\left(\frac{\nabla h}{|\nabla h|} + g|\nabla h|\nabla h\right)}, \tag{5}$$

below the roughening transition; $\beta = (k_B T)^{-1}$. For $g = 0$, PDE (5) becomes

$$\partial_t h = \Delta e^{-\beta \operatorname{div}\left(\frac{\nabla h}{|\nabla h|}\right)}. \tag{6}$$

Here, we set the material parameter $D_s \varrho^0$ equal to unity; alternatively, this parameter, $D_s \varrho^0$, can be absorbed in the scaling of the time variable. In a similar vein, the parameter γ is eliminated in (5) by suitable scaling of the spatial coordinates or the Boltzmann energy, $k_B T$. Note that a simplified version of PDE (5) comes from linearizing the exponential of the Gibbs–Thomson relation, $\varrho_s \approx \varrho^0(1 + \beta\mu_s)$, under the typical assumption that the chemical potential, μ_s, has magnitude sufficiently smaller than $k_B T$ [10].

1.2. Relevant microscopic models

The derivation of PDE (5) is expected to hold away for facets [6]. This PDE is plausibly linked to: (a) the BCF model of step flow on monotone step trains [5,6,28]; and (b) a family of atomistic models [8]. Here, we outline elements of these microscale theories. In Section 2, we provide a more detailed review of their linkages to (5).

First, consider the mesoscale picture of step flow. The BCF model accounts for diffusion of adatoms and attachment/detachment of atoms at steps [5]. Key ingredients of the respective formalism are: (i) a step velocity law by mass conservation; (ii) a diffusion equation for adatoms on each nanoscale domain, terrace, between steps; and (iii) a Robin boundary condition for the adatom density at the step edge. Hence, the step is viewed as a free boundary for a Stefan-type problem; the step position is determined via diffusion and each terrace is a level set for the height. In the kinetic regime of diffusion-limited kinetics, the Robin boundary condition reduces to a Dirichlet condition [5]. In the continuum limit, the step height, which is equal to the vertical lattice spacing, approaches zero while the surface slope is kept fixed.

Alternatively, in the respective atomistic picture based on the SOS model, the core mechanism is the hopping of atoms on the crystal lattice [8,38]. The formalism relies on a Markovian process representing the motion of each atom from one lattice site to a neighboring site. In this model, the transitions between atomistic configurations are determined by Arrhenius rates which in turn are related to the number of bonds that each atom would be required to break in order to move. In [8], a macroscopic limit of these dynamics, as the lattice spacing vanishes, is proposed via the form of the surface tension as the p-Laplacian for the potential $V(x) = |x|^p$, $p > 1$. PDE (5) is an extension of that macroscopic limit in [8] to $p = 1$. Notably, the resulting PDE is sensitive to the way by which the initial height profile is scaled [8].

1.3. Our mathematical approach and core result

Our mathematical approach makes use of a version of the subgradient formalism [22], adapted to the exponential, fourth-order PDE (5). In physical terms, intuitively, this formalism may be viewed as tantamount to a limiting procedure by which the facet is artificially smoothed out and then is allowed to approach a flat plateau. This procedure can be viewed as the outcome of the regularization of the surface free energy, $E[h]$; see, e.g., [18,24]. It should be noted that a different approach of regularization found in the literature relies on the truncation of Fourier series expansions for the height profile, which yields nonlinear differential equations for the requisite coefficients [13,21,39].

Our construction of a solution treats the facet edge as a free boundary, in the spirit of [40]. In the continuum thermodynamics framework, the boundary conditions at the facet edge result from the extended-gradient formalism as follows. Replace PDE (5) by the statement that $\partial_t h$ *picks* the subgradient of $E[h]$ with the minimal norm in the appropriate metric; see, e.g., [23,41] for works on the H^{-1} gradient flow. In particular, in $1 + 1$ dimensions PDE (6) is written as

$$\begin{aligned}\partial_t h &= -\partial_x\left[e^{-\partial_x\left(\frac{\partial_x h}{|\partial_x h|}\right)}\partial_{xx}\left(\frac{\partial_x h}{|\partial_x h|}\right)\right] \\ &= \partial_x\left[e^{-\partial_x\left(\frac{\partial_x h}{|\partial_x h|}\right)}\partial_x\left(\frac{\delta E}{\delta h}\right)\right].\end{aligned}$$

This evolution can be viewed as the nonlinear (weighted) H^{-1}-gradient flow with (exponential) mobility equal to $e^{-\partial_x\left(\frac{\partial_x h}{|\partial_x h|}\right)}$ for the free energy functional $E[h]$ given by (1) with $g = 0$; see Appendix for a discussion. We write

$$\partial_t h = \partial_{xxx} v \quad \text{where} \quad \partial_x v = e^{-\partial_x w},$$

where $w = h_x/|h_x|$, $-\partial_x w \in \partial_{L^2} E$ is an element of the L^2-subdifferential of $E[h]$, and the function $v(x)$ is determined in the sense described in Section 3. The functions v and $\partial_x v$ are continuous; in addition, these functions are subject to the symmetry of the surface profile. Thus, $-\partial_x w = \mu$, the continuum-scale step chemical potential, and w are continuous across the facet. Furthermore, the mass conservation statement $\partial_t h + \partial_x J = 0$ where $J = -\partial_{xx} v$ is the x-component of the (vector-valued) adatom flux $\mathbf{J}$, entails a jump condition for the continuum-scale adatom flux and height across the facet edge [25]. It should be borne in mind that the facet height, h_f, is constant in x; thus, the above conditions can be applied by successive integrations with respect to x of the conservation law for the height, where $\partial_t h$ in the facet region is the vertical facet speed, $\dot{h}_f$.

For $g = 0$, i.e., if step–step interactions are neglected, this procedure entails a discontinuous height and mass flux at the facet boundary, in agreement with rigorous studies in [25] on the total variation flow model

$$\partial_t h = -\partial_x^3\left(\frac{\partial_x h}{|\partial_x h|}\right) = \partial_x^2\left(\frac{\delta E}{\delta h}\right), \tag{7}$$

which has the structure of a (non-weighted) H^{-1} gradient flow. The reader is referred to [35,42] for related works in the presence of elasticity.

A noteworthy result here is the derivation of a system of two differential equations for the facet position, x_f, and facet height, h_f, via the exponential PDE. By properties of this system, we infer that facets in convex and concave parts of the surface *behave differently*. In particular, by our theory, if the initial height profile is sinusoidal, the surface peaks immediately break into expanding facets; in contrast, no facets form at the valleys of the initial profile (see Section 4). It should be mentioned that experimental observations in epitaxial relaxation do not seem to report the formation of asymmetric facets of one-dimensional corrugations, although lack of symmetry in facet dynamics is observed in two spatial dimensions in a certain temperature range [16].

1.4. Limitations

Our work points to several open questions. First, the precise nature of the gradient flow for PDE (5) is not adequately understood. As noted earlier, the comparison of our continuum predictions to results from the step flow near facets is an interesting problem left for future research. A requisite issue in this context is the sign of the interactions between colliding steps on facets [17]. In a similar vein, we do not pursue comparisons of the continuum predictions against KMC simulations, which would connect the PDE solution to atomistic dynamics; see [8]. Our construction of an explicit solution to the exponential PDE focuses on one spatial coordinate with diffusion-limited kinetics and $g = 0$. In 2+1 dimensions or settings with elasticity or other kinetics (say, attachment–detachment limited kinetics), the subgradient formalism becomes more intricate. The facet evolution in such cases needs to be further studied.

1.5. Paper outline

The remainder of this paper is organized as follows. In Section 2, we review linkages of PDE (5) to existing microscopic models. Section 3 focuses on the construction of the ODEs governing facet dynamics. In Section 4, we numerically solve both the ODE system and an appropriately regularized version of the PDE; and compare the outcomes. Finally, in Section 5, we summarize the results obtained and outline some topics for future work.

2. Mesoscale and atomistic descriptions: A review

In this section, we describe ingredients of the mesoscale and atomistic models that motivate the study of (5) as a hydrodynamic-type limit. In particular, we review basics of the BCF model [5] and a heuristic derivation of its continuum limit assuming that this limit exists (Section 2.1). We also outline the relevance to the exponential PDE of a kinetic Monte Carlo model of crystal surface relaxation [8] (Section 2.2). The emergence of the BCF description of step flow from atomistic dynamics is not addressed here; see, e.g., [43].

2.1. BCF model and its continuum limit

By the BCF model [5], the crystal surface consists of atomic steps separated by nanoscale terraces. In this subsection, we review the basic elements of step flow, needed for our purposes, by mainly following the formalism of [6,44].

Fig. 1 depicts the top view of descending, non-intersecting steps of atomic height a in two dimensions. The steps surround a top terrace. The projections of the step edges onto a fixed, high-symmetry reference plane (xy-plane, with position vector $\mathbf{r}$) are modeled by a family of smooth curves, numbered by i ($i = 1, 2, \ldots, N$)

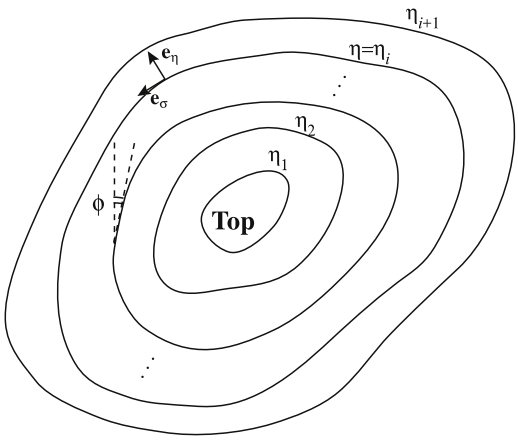

Fig. 1. Geometry of monotone step train in 2+1 dimensions (top view). In curvilinear coordinates (η, σ), the depicted contours are projections of descending steps onto a fixed reference plane; $\eta = \eta_i$ at the ith edge while σ varies along a step edge. The step orientation, relative to a fixed axis, is indicated by the (local) angle ϕ.

relative to the top terrace where $N \gg 1$. These curves are described by the position vector $\mathbf{r}(\eta, \sigma; t)$, where η and σ are viewed as Lagrangian coordinates. In general, the ith step is defined as the set $\{\mathbf{r}(\eta_i, \sigma; t) : 0 \le \sigma < 2\pi\}$, and the ith terrace is given as the region $\{\mathbf{r}(\eta, \sigma; t) : \eta_i < \eta < \eta_{i+1},\ 0 \le \sigma < 2\pi\}$. In the special case of radial geometry, when the steps are concentric circles, the variable η corresponds to the polar coordinate for the distance from the origin. The variable σ corresponds to the angle in polar coordinates and increases counterclockwise. In general, the unit vectors normal and parallel to step edges in the direction of increasing η and σ are denoted $\mathbf{e}_\eta$ and $\mathbf{e}_\sigma$, where we take $\mathbf{e}_\eta \cdot \mathbf{e}_\sigma = 0$. The corresponding metric coefficients are

$$\xi_\eta = |\partial_\eta \mathbf{r}|, \quad \xi_\sigma = |\partial_\sigma \mathbf{r}|, \tag{8}$$

with the convention that $\partial_\eta \mathbf{r} = \xi_\eta \mathbf{e}_\eta$ and $\partial_\sigma \mathbf{r} = \xi_\sigma \mathbf{e}_\sigma$.

The surface height, $h(\mathbf{r}(\eta, \sigma; t), t)$, is a function of η only and obeys

$$h|_{\eta=\eta_{i+1}} - h|_{\eta=\eta_i} = -a.$$

In the continuum limit, we let $a \downarrow 0$ while we keep the slope fixed. The Taylor expansion of the left-hand side of the last equation entails that $a/(\xi_\eta(\delta\eta)_i)$ approaches the positive slope $-(\partial_\perp h)|_{\eta=\eta_i} = |\nabla h|$ as $a \downarrow 0$, and $(\delta\eta)_i := \eta_{i+1} - \eta_i = \mathcal{O}(a)$ so that the slope is kept fixed. Note that $\partial_\perp := \xi_\eta^{-1}\partial_\eta$.

2.1.1. Laws of step flow and continuum limit

The main assumptions of the step flow model are: (i) The steps move by mass conservation through attachment/detachment of adatoms at each step edge with kinetic rate k; and (ii) the adatoms diffuse on each terrace in the quasi-steady regime, i.e., the density of adatoms, ϱ_i, on the ith terrace reaches the steady state much faster than the motion of steps. Thus, $D_s \Delta \varrho_i = \partial_t \varrho_i \approx 0$ for $\eta_i < \eta < \eta_{i+1}$, where D_s is the terrace diffusivity. In addition, we assume that the continuum limit, as $a \to 0$, of step flow exists. In this limit, we treat the parameter $D_s/(ka)$ as constant.

By mass conservation, the normal velocity of the ith step is given by

$$v_{i,\perp} = a^{-1}(J_{i-1,\perp} - J_{i,\perp}) \qquad \text{at } (\eta_i, \sigma). \tag{9}$$

Here, $J_{i,\perp}(\mathbf{r}(\eta, \sigma; t), t) = \mathbf{e}_\eta \cdot \mathbf{J}_i(\mathbf{r}(\eta, \sigma; t), t)$ where $\mathbf{J}_i = -D_s \nabla \varrho_i$ is the vector-valued adatom flux on the ith terrace. By slight abuse of notation, we also write $J_{i,\perp}(\eta, \sigma) = J_{i,\perp}(\mathbf{r}(\eta, \sigma; t), t)$ when no confusion occurs; and ditto for ϱ_i.

In the continuum limit, as $a \downarrow 0$, (9) reduces to a mass conservation statement. Indeed, the $v_{i,\perp}$ approaches $\partial_t h/|\nabla h|$ at (η_i, σ). Furthermore, by Taylor expanding $J_{i,\perp}(\eta, \sigma)$ on the ith terrace (for $\eta_i < \eta < \eta_{i+1}$) as $\eta \uparrow \eta_{i+1}$ in terms of the value of $J_{i,\perp}(\eta, \sigma)$ at $\eta = \eta_i$ (i.e., the value obtained by $\eta \downarrow \eta_i$), we have

$$J_{i,\perp}(\eta_i, \sigma) \approx J_{i,\perp}(\eta_{i+1}, \sigma) - (\delta\eta)_i \partial_\eta J_{i,\perp}(\eta_i, \sigma).$$

Then, we apply the quasi-steady approximation, $\mathrm{div}\mathbf{J}_i \approx 0$ on the ith terrace, which gives $\xi_\eta^{-1}\partial_\eta J_{i,\perp}(\eta, \sigma) + \xi_\sigma^{-1}\partial_\sigma J_{i,\parallel}(\eta, \sigma) \approx 0$ for $\eta_i < \eta < \eta_{i+1}$, and allow η to approach η_i on the ith terrace ($\eta \downarrow \eta_i$). Thus, we obtain

$$J_{i,\perp}(\eta_i, \sigma) \approx J_{i,\perp}(\eta_{i+1}, \sigma) + (\xi_\eta(\delta\eta)_i)\xi_\sigma^{-1}\partial_\sigma J_{i,\parallel}(\eta_i, \sigma).$$

Here, $J_{i,\parallel}(\eta, \sigma) = \mathbf{e}_\sigma \cdot \mathbf{J}_i(\eta, \sigma)$ on the ith terrace. Hence, the right-hand side of (9) approximately reads

$$\begin{aligned} v_{i,\perp} &\approx a^{-1}\{J_{i-1,\perp}(\eta_i, \sigma) - J_{i,\perp}(\eta_{i+1}, \sigma) - (\xi_\eta(\delta\eta)_i)\xi_\sigma^{-1}\partial_\sigma J_{i,\parallel}(\eta_i, \sigma)\} \\ &\approx a^{-1}\{-(\delta\eta)_i\, \partial_\eta J_\perp(\eta_i, \sigma) - (\xi_\eta(\delta\eta)_i)\xi_\sigma^{-1}\partial_\sigma J_{i,\parallel}(\eta_i, \sigma)\} \\ &= -a^{-1}(\xi_\eta(\delta\eta)_i)\{\xi_\eta^{-1}\partial_\eta J_\perp(\eta_i, \sigma) + \xi_\sigma^{-1}\partial_\sigma J_\parallel(\eta_i, \sigma)\}, \end{aligned}$$

which is identified with $-|\nabla h|^{-1}\mathrm{div}\mathbf{J}$ in the continuum limit. In this derivation, the continuum-scale flux, $\mathbf{J}(\mathbf{r}, t)$, is defined as the limit of $\mathbf{J}_{i-1}(\eta_i, \sigma)$ as $a \to 0$, with $J_\perp = \mathbf{e}_\eta \cdot \mathbf{J}$ and $J_\parallel = \mathbf{e}_\sigma \cdot \mathbf{J}$. Therefore, we obtain conservation statement (4), viz.,

$$\partial_t h = -\mathrm{div}\mathbf{J}.$$

Next, we consider the attachment/detachment of atoms at steps. By the quasi-steady approximation, we set $D_s \Delta\varrho_i = \partial_t \varrho_i \approx 0$ on the ith terrace. The boundary conditions for this diffusion equation are of the Robin type, viz.,

$$\begin{aligned} -J_{i,\perp} &= k(\varrho_i^+ - \varrho_i^{\mathrm{eq}}) \quad \text{at } (\eta_i, \sigma), \\ J_{i,\perp} &= k(\varrho_i^- - \varrho_{i+1}^{\mathrm{eq}}) \quad \text{at } (\eta_{i+1}, \sigma'), \end{aligned} \tag{10}$$

where k is the attachment–detachment rate and $\varrho_i^\pm$ is the restriction of ϱ_i at a step edge as η approaches $\eta_i\,(+)$ or $\eta_{i+1}\,(-)$ on the ith terrace. The quantity ϱ_i^{eq} is the equilibrium adatom density at the ith step and is given by the Gibbs–Thomson relation (discussed below). This ϱ_i^{eq} is strictly defined on each step, incorporates the thermodynamics of each step, e.g., elastic step–step interactions, and is in principle distinct from the restrictions at the ith edge of the (steady-state) adatom densities, ϱ_i and ϱ_{i-1}, defined on the adjacent terraces. Eqs. (10) are combined for $\sigma \neq \sigma'$ to yield

$$\begin{aligned} J_{i,\perp}(\eta_i, \sigma) + J_{i,\perp}(\eta_{i+1}, \sigma') &= k[\varrho_i(\eta_{i+1}, \sigma') - \varrho_i(\eta_i, \sigma)] \\ &\quad - k[\varrho_{i+1}^{\mathrm{eq}}(\sigma') - \varrho_i^{\mathrm{eq}}(\sigma)]. \end{aligned}$$

We now show that, in the limit $\delta\sigma := \sigma' - \sigma \to 0$ and $(\delta\eta)_i \downarrow 0$, the last equation heuristically entails a Fick-type law for continuum-scale flux, $\mathbf{J} = (J_\perp, J_\parallel)$, in terms of the continuum-scale equilibrium density, ϱ^{eq}. This density is defined on the high-symmetry (xy-) plane as the limit of ϱ_i^{eq}, considered as a function of η_i and σ, when $(\delta\eta)_i \downarrow 0$. Recall that $(\delta\eta)_i$ is $\mathcal{O}(a)$ as $a \downarrow 0$, because the slope is kept fixed; thus, the limits $a \downarrow 0$ and $(\delta\eta)_i \downarrow 0$ are taken simultaneously while $a/(\delta\eta)_i$ is kept fixed. On the other hand, $\delta\sigma$ is allowed to approach zero independently of a. Next, consider the Taylor expansion

$$\begin{aligned} &\varrho_i(\eta_{i+1}, \sigma') - \varrho_i(\eta_i, \sigma) \approx (\delta\eta)_i\, \partial_\eta \varrho_i + (\delta\sigma)\partial_\sigma \varrho_i \\ &= -(\xi_\eta(\delta\eta)_i)D_s^{-1}J_{i,\perp} - (\xi_\sigma(\delta\sigma))D_s^{-1}J_{i,\parallel} \text{ at } (\eta_i, \sigma), \end{aligned}$$

where we used the definitions of the adatom flux components, $J_{i,\perp} = -D_s(\xi_\eta^{-1}\partial_\eta \varrho_i)$ and $J_{i,\parallel} = -D_s(\xi_\sigma^{-1}\partial_\sigma \varrho_i)$, on the ith terrace. By anticipating the continuum limit, we set

$$\begin{aligned} &J_{i,\perp}(\eta_i, \sigma) \approx J_\perp(\eta, \sigma),\ J_{i+1,\perp}(\eta_{i+1}, \sigma') \approx J_\perp(\eta', \sigma'), \\ &\varrho_i^{\mathrm{eq}}(\sigma) \approx \varrho^{\mathrm{eq}}(\eta, \sigma),\ \varrho_{i+1}^{\mathrm{eq}}(\sigma') \approx \varrho^{\mathrm{eq}}(\eta', \sigma'), \end{aligned} \tag{11}$$

for some η and η'. In addition, we set $a\{\xi_\eta(\delta\eta)_i\}^{-1} \approx m(\eta, \sigma)$ which should approach the positive surface slope, $|\nabla h|$, at (η, σ). This approximation allows us to replace $\xi_\eta(\delta\eta)_i$ by a/m. Furthermore, we consider the Taylor expansion

$$\begin{aligned} \varrho_{i+1}^{\mathrm{eq}}(\sigma') - \varrho_i^{\mathrm{eq}}(\sigma) &\approx \varrho^{\mathrm{eq}}(\eta', \sigma') - \varrho^{\mathrm{eq}}(\eta, \sigma) \\ &\approx (\partial_\eta \varrho^{\mathrm{eq}})(\delta\eta) + (\partial_\sigma \varrho^{\mathrm{eq}})(\delta\sigma) \text{ at } (\eta, \sigma) \end{aligned}$$

where $\delta\eta = \eta' - \eta$. Let us assume that [6]

$$\wp := \frac{D_s}{ka} = \mathcal{O}(1) \quad \text{as } a \downarrow 0,$$

so that this parameter can be treated as constant in the continuum limit. Hence, from boundary conditions (10) we obtain the expression

$$\begin{aligned} &a\left\{\left(2 + \frac{1}{\wp m}\right)J_\perp + \frac{(\xi_\eta(\delta\eta))}{a}\frac{D_s}{\wp}(\xi_\eta^{-1}\partial_\eta \varrho^{\mathrm{eq}})\right\} \\ &+ \frac{(\xi_\sigma(\delta\sigma))}{\wp}\left\{J_\parallel + D_s(\xi_\sigma^{-1}\partial_\sigma \varrho^{\mathrm{eq}})\right\} = 0 \end{aligned}$$

at the point (η, σ) (where $|\nabla h| \neq 0$). In this expression, we can allow $a \downarrow 0$ with $\delta\sigma \neq 0$; or, alternatively, set $\delta\sigma = 0$ with $a \neq 0$, treating a and $\delta\sigma$ as independent from each other. Note that the dimensionless parameter $(\xi_\eta(\delta\eta))/a$, which enters the above expression, can be replaced by $1/m$ and approaches $|\nabla h|^{-1}$. Hence, we extract the formulas

$$J_\perp = -\frac{D_s}{1 + \dfrac{2D_s}{ka}|\nabla h|}(\xi_\eta^{-1}\partial_\eta \varrho^{\mathrm{eq}}), \quad J_\parallel = -D_s(\xi_\sigma^{-1}\partial_\sigma \varrho^{\mathrm{eq}}), \tag{12a}$$

in the local coordinate system. Setting $\partial_\perp = \xi_\eta^{-1}\partial_\eta$ and $\partial_\parallel = \xi_\sigma^{-1}\partial_\sigma$, we find that the above flux components are in agreement with the corresponding formulas derived in [6] by a different method, namely, the approximate solution of the diffusion equation via the separation of length scales into fast and slow on each terrace. In particular, for diffusion-limited kinetics, when the diffusion of adatoms on terraces is the slowest process, the length D_s/k is much smaller than the terrace size, $[D_s/(ka)]|\nabla h| \ll 1$; thus, by (12a) we find

$$J_\perp = -D_s(\xi_\eta^{-1}\partial_\eta \varrho^{\mathrm{eq}}), \quad J_\parallel = -D_s(\xi_\sigma^{-1}\partial_\sigma \varrho^{\mathrm{eq}}) \quad \text{if} \quad \frac{D_s}{ka}|\nabla h| \ll 1. \tag{12b}$$

Therefore, $\mathbf{J} = J_\perp \mathbf{e}_\eta + J_\parallel \mathbf{e}_\sigma = -D_s \nabla \varrho^{\mathrm{eq}}$, as expected by the typical Fick law of diffusion [6]; cf. (3) where ϱ_s is identified with ϱ^{eq}.

Eqs. (4) and (12) need to be complemented with a formula for ϱ^{eq} involving the continuum-scale step chemical potential, μ_s. At the level of step flow, the Gibbs–Thomson relation dictates that

$$\varrho_i^{\mathrm{eq}} = \varrho^0 e^{\frac{\mu_i}{k_B T}}, \tag{13}$$

where ϱ^0 is a reference density for an atomically flat terrace. The step chemical potential, $\mu_i(\sigma)$, of the ith step is defined as the change of the step energy by addition or removal of an atom to or from the step edge at $\eta = \eta_i$. Following [6], consider a short step length, $\mathrm{d}s = \xi_\sigma \mathrm{d}\sigma$, of the ith edge that has energy $\mathcal{U}_i \mathrm{d}s$ at (η_i, σ); $\mathcal{U}_i$ is the step energy per unit length. The exchange of atoms with the step edge results in the motion of the step along its local normal by distance $\mathrm{d}r = \xi_\eta \mathrm{d}\eta$ where $\mathrm{d}\eta$ is the respective shift of η_i. Hence, the step energy $\mathcal{U}_i \mathrm{d}s$ changes by $\mathrm{d}_\eta(\mathcal{U}_i\, \mathrm{d}\sigma)$, where the shift operator d_η is defined by $\mathrm{d}_\eta Q := Q|_{\eta+\mathrm{d}\eta} - Q|_\eta$. Accordingly, we write

$$\mu_i = \frac{1}{a}\frac{\mathrm{d}_\eta(\mathcal{U}_i \mathrm{d}s)}{\mathrm{d}r \mathrm{d}s} = \frac{1}{a}\{\xi_\eta^{-1}\partial_{\eta_i}\mathcal{U}_i + \mathcal{U}_i(\xi_\eta \xi_\sigma)^{-1}\partial_\eta \xi_\sigma\} \quad \text{at } \eta = \eta_i. \tag{14}$$

By using the elementary formula $\xi_\eta^{-1}\partial_\eta \xi_\sigma = \kappa \xi_\sigma$ where κ is the curvature of the curve $\mathbf{r}(\eta, \sigma; t)$ with $\eta = \text{const.}$, we obtain

$$\mu_i = \frac{1}{a}\left(\kappa_i \mathcal{U}_i + \xi_{\eta_i}^{-1}\partial_{\eta_i}\mathcal{U}_i\right). \tag{15}$$

The quantity $\mathcal{U}_i$ incorporates the step line tension, $\tilde{\gamma}_i$, which is the energy cost per unit length to create a step and may in principle depend on the step orientation ϕ (see Fig. 1), as well as the step–step interaction contribution, $\mathcal{U}_i^{\rm int}$. In a simple scenario for homoepitaxy, $\tilde{\gamma}_i = \gamma a$ is a global, material-dependent constant; and step interactions are modeled as nearest-neighbor repulsions [33,45], viz.,

$$\mathcal{U}_i = a\gamma + \mathcal{U}_i^{\rm int}, \quad \mathcal{U}_i^{\rm int} = \tilde{g}\,(V_{i,i+1} + V_{i,i-1}), \tag{16}$$

where $\tilde{g}$ is the interaction strength (energy/length), and $V_{i,i\pm1}$ amounts to the interaction between the ith and $(i \pm 1)$th steps and depends on η_i and $\eta_{i\pm1}$. For elastic-dipole or entropic interactions, the $V_{i,j}$ $(j = i \pm 1)$ is taken to be [6]

$$V_{i,i+1} = \frac{1}{3} m_i^2 \Phi(r_i, r_{i+1}), \quad V_{i,i-1} = \frac{1}{3} m_{i-1}^2 \Phi(r_i, r_{i-1}),$$

where

$$m_i := \frac{a}{r_{i+1} - r_i}; \quad r_i = r|_{\eta=\eta_i}, \quad r = \int_{\eta_0}^{\eta} \xi_{\eta'}\, {\rm d}\eta',$$

and $\Phi(\zeta, \chi)$ is a geometrical factor described in some detail in [6].

In the continuum limit, the curvature κ_i of the step approaches $-{\rm div}[\nabla h/|\nabla h|]$ at the point (η_i, σ). By (15), the step chemical potential, μ_i, approaches form (2) under mild assumptions for Φ. The interested reader is referred to [6].

Note that in the attachment–detachment-limited regime, where

$$\frac{D_s}{ka}|\nabla h| \gg 1,$$

the attachment/detachment of atoms at steps is the slowest process. In this case, the resulting PDE in 1+1 dimensions acquires a slope-dependent, extra mobility, viz.,

$$\partial_t h = \partial_x \left[\frac{1}{|\partial_x h|} \partial_x e^{-\beta \partial_x \left(\frac{\partial_x h}{|\partial_x h|} + g|\partial_x h|\partial_x h \right)} \right]. \tag{17}$$

The study of this PDE lies beyond our present scope.

2.2. Broken-bond model and hydrodynamic limit

In this subsection, we review aspects of the emergence of continuum laws from atomistic principles in [8]. Motivated by an adatom model proposed in [7] and studies of hydrodynamic limits undertaken in [46–48], the authors in [8] derive exponential PDEs of form similar to (5). This atomistic formulation views the crystal surface as a function $h_N(\alpha, t)$ for time $t \geq 0$ and position $\alpha \in \mathbb{T}_N^d = (\mathbb{Z}/N\mathbb{Z})^d$ on the periodic lattice, with values of h_N in the set of integers, $\mathbb{Z}$; d is the spatial dimension. The rates are related to an interaction potential, $V : \mathbb{Z} \to \mathbb{R}$, taken to be the non-negative, strictly convex, symmetric function, $V(z) = |z|^p$, of the discrete slope, z. The choice for V made in [8], and the most common choice in the literature on the physics of crystal surfaces, is $V(z) = |z|$ (if $p = 1$), which amounts to bond breaking by the SOS model [38].

From such an interaction potential, $V = |z|^p$, in [8] a family of Arrhenius rates are proposed based upon a generalized coordination number. One can think of the generalized coordination number as the (symmetrized) energy cost associated with removing a single atom from site α on the crystal surface, where the energy is determined by summing over the interaction potential evaluated on local fluxes.

In [8], two scaling limits are studied. First, for $p \geq 1$, the evolution of the height of a smooth crystal surface is found to be

$$\partial_t h = -\frac{1}{2d} \Delta({\rm div}(\nabla \sigma_D(\nabla h))), \tag{18}$$

where $\nabla\sigma_D : \mathbb{R}^d \to \mathbb{R}^d$ is the gradient of the surface tension, σ_D, which is a convex function determined by a free-energy computation and depends on the choice of the interaction potential, V. The definition of this σ_D arises from essentially applying the local Gibbs measure (local equilibrium) for finding non-equilibrium dynamics in the microscopic model of crystal surface evolution [8]. In particular, σ_D stems from using a discrete chemical potential, which matches well the macroscopic dynamics; see [8]. PDE (18) arises from a smooth diffusion scaling limit of the form $\bar{h}_N(x, t) = N^{-1} h(\alpha, N^4 t)$ with $Nx \in [\alpha - 1/2, \alpha + 1/2)$.

Similarly, in [8], a second PDE for a rough crystal evolution is proposed for $p > 1$ with fixed temperature β^{-1} $(\beta > 0)$, viz.,

$$\partial_t h = \frac{1}{2d} \Delta \left(e^{-{\rm div}(\nabla \sigma_C(\nabla \bar{h}))} \right); \quad \sigma_C(z) = \lim_{\kappa \to \infty} \kappa^{-p} \sigma_D(\kappa z). \tag{19}$$

The form that the surface tension then takes is the p-Laplacian for $\sigma_C(z) = \beta|z|^p$, resulting in the evolution

$$\partial_t h = \frac{1}{2d} \Delta \left(e^{-\beta {\rm div}\left((|\nabla h|^{p-2} \nabla h) \right)} \right). \tag{20}$$

This PDE arises from a rough scaling limit of the form $\bar{h}_N(x, t) = N^{-q} h(\alpha, N^{q+2} t)$ with $Nx \in [\alpha - 1/2, \alpha + 1/2)$ and $q = p/(p-1)$.

However, the rough scaling when $p = 1$ can be adapted by formally following the derivation in [8, Section 6.2], if one systematically lowers the temperature, β^{-1}, as one increases the system size ($\beta = \beta(N)$ such that $\beta(N) \to \infty$ as $N \to \infty$). Then, the methods of [8] can be invoked to derive (5) with Boltzmann constant $\tilde{\beta}$, and, for instance, $q = 1$ and $\beta(N) = \tilde{\beta} N$.

3. ODE system for facet motion via exponential PDE

In this section, we formulate an ODE system for facets in a periodic surface corrugation with $g = 0$ (no elasticity) in 1+1 dimensions. This amounts to the construction of a solution for the height profile. We first discuss a general framework for the gradient flow. Accordingly, we analytically indicate the different behaviors of top and bottom facets by use of the ODEs. For algebraic convenience, we use PDE (6) by setting β equal to unity, absorbing β into the spatial coordinates. In Section 4, our construction of a solution is compared to numerics for the PDE by regularization of the surface free energy, $E[h]$.

In the case with the (non-weighted) H^{-1}-total variation flow (e.g. [25–27]), the PDE takes the form

$$\partial_t h = -\partial_{xx} \partial_x \left(\frac{\partial_x h}{|\partial_x h|} \right), \quad h(x, 0) = h_0(x), \tag{21}$$

where $h_0(x)$ is assumed to be symmetric and have an extremum at $x = 0$. A weak solution to (21) is derived in [25] as a facet solution (symmetric about the maximum or minimum of h_0 at $x = 0$) near the critical point $x = 0$ of h_0. This weak solution has the form

$$h(x, t) = \begin{cases} h_f(t) & \text{for } x < x_f(t), \\ h_0(x) & \text{for } x > x_f(t), \end{cases}$$

where $x = x_f(t)$ is the facet position and $h_f(t)$ is the facet height. The dynamics for $(x_f(t), h_f(t))$ obey the ODE system

$$\begin{cases} \dot{h}_f(t) = -3 x_f(t)^{-3}, \\ \dot{x}_f(t)(h_0(x_f) - h_f(t)) = -3 x_f(t)^{-2}. \end{cases} \tag{22}$$

This is the symmetric formulation for the H^{-1}-total variation flow. For the case of the L^2 total variation flow, in which the PDE for h is of second order, see, e.g., [22].

We now turn our attention to simplified exponential PDE (6). For this case, we lack a mathematically rigorous theory. Following the works of [25–27], we recognize that (6) can be realized as the weighted H^{-1}-gradient flow, with mobility $e^{-\partial_x \left(\frac{\partial_x h}{|\partial_x h|} \right)}$, for the

respective free energy functional $E[h]$ of (1) with $g = 0$. For the convenience of the reader, a formal discussion of the weighted H^{-1}-gradient flow with (nonlinear) mobility is provided in Appendix. Note that PDE (6) is written as

$$\partial_t h = -\partial_x \left[e^{-\partial_x \left(\frac{\partial_x h}{|\partial_x h|} \right)} \partial_{xx} \left(\frac{\partial_x h}{|\partial_x h|} \right) \right] = \partial_x \left[e^{-\partial_x \left(\frac{\partial_x h}{|\partial_x h|} \right)} \partial_x \left(\frac{\delta E}{\delta h} \right) \right],$$

where the variational derivative $\delta E/\delta h$ is defined in the sense of L^2. *This model of evolution implies an asymmetry between convex and concave parts of the crystal surface, as demonstrated below.*

3.1. ODE dynamics from subdifferential formulation

In view of the above formalism, we proceed to derive ODEs for facet motion in the exponential total variation flow

$$\partial_t h = \partial_{xx} e^{-\partial_x \left(\frac{\partial_x h}{|\partial_x h|} \right)}, \quad h(x,0) = h_0(x), \tag{23}$$

using the natural profile stemming from a regularized solution for the 1-Laplacian.

Evidently, PDE (23) has the structure

$$\begin{aligned} &\partial_t h = -\partial_x J \quad \text{(continuity equation)},\\ &J = -\partial_x \varrho^{\mathrm{eq}} \quad \text{(Fick's law)},\\ &\varrho^{\mathrm{eq}} = e^{\mu} \quad \text{(Gibbs–Thomson relation)},\\ &\mu = \frac{\delta E}{\delta h} = -\partial_x w(\partial_x h) \quad \text{(thermodynamic force)}, \end{aligned}$$

where J is the (scalar) mass flux, μ is the continuum-scale step chemical potential, ϱ^{eq} is the equilibrium adatom density, and $w(u) = u/|u|$ (see also Assumption A4 below).

We spell out the following simplifying symmetry assumptions (a few of which we have already mentioned above):

- A1. The height solution is symmetric (with respect to $x = 0$), i.e., $h(-x,t) = h(x,t)$.
- A2. The facet has zero slope, i.e., $\partial_x h = 0$ for $x \in (-x_f, x_f)$. In addition, for a top facet we have $\partial_x h < 0$ when $x > x_f$, and for a bottom facet we have $\partial_x h > 0$ when $x > x_f$.
- A3. The vertical speed of the top facet is negative, $\dot{h}_f < 0$; and the vertical speed of the bottom facet is positive, $\dot{h}_f > 0$.
- A4. The function $w(u) = u/|u|$ (u is the slope) is extended onto the facet as an odd function on $\mathbb{R}$. We set $\tilde{w}(x,t) = w(\partial_x h)$.
- A5. The mass flux $J(x,t)$ is an odd function on $\mathbb{R}$, i.e., $J(-x,t) = -J(x,t)$.

In view of Assumption A1, it suffices to consider $x > 0$. On the facet, where $0 < x < x_f(t)$ and $h(x,t) = h_f(t)$ (by Assumption A2), we therefore obtain

$$\dot{h}_f = -\partial_x J,$$

which by integration yields

$$J(x,t) = -x\dot{h}_f + C_1(t).$$

Note that $C_1(t) = 0$ by the symmetry consideration that J will be odd (by Assumption A5). In addition, as in the total variation flow observations of [25], we are compelled to recognize a jump in h at $x = x_f(t)$, forcing the remaining functions J and μ to have continuous derivatives.

By the PDE structure, we additionally have

$$\partial_x(e^{\mu}) = -J(x,t),$$

which entails

$$\mu(x,t) = \ln\left(\frac{x^2}{2}\dot{h}_f + C_2(t) \right).$$

We also have

$$\partial_x \tilde{w} = -\ln\left(\frac{x^2}{2}\dot{h}_f + C_2(t) \right),$$

which is integrated to give

$$\tilde{w}(x,t) = -\int_0^x \ln\left(\frac{s^2}{2}\dot{h}_f + C_2(t) \right) \mathrm{d}s + C_3(t).$$

The integration constant $C_3(t)$ is determined by our assumption that $\tilde{w}(x,t)$ is an odd function of x (Assumption A4); hence, $C_3 = 0$.

In addition, mass conservation dictates that

$$\int_0^{x_f} h_0(s)ds = h_f x_f,$$

which yields the motion law

$$\dot{x}_f(h_0(x_f) - h_f) = \dot{h}_f x_f. \tag{24}$$

3.2. Dynamics of top facet

At this stage, we need to specify if the symmetric facet lies in the convex or concave part of the surface. This choice affects the sign of $\dot{h}_f$ and leads to different dynamics as we discuss below. Let us begin with the case in which the facet is a degenerate local maximum. In this case, $\dot{h}_f < 0$ by Assumption A3.

By continuity of w and μ, the following conditions hold:

$$\tilde{w}(x_f,t) = -\int_0^{x_f} \ln\left(\frac{s^2}{2}\dot{h}_f + C_2(t) \right) \mathrm{d}s = -1,$$

$$\mu(x_f,t) = \ln\left(\frac{x_f^2}{2}\dot{h}_f + C_2(t) \right) = 0.$$

The condition for μ yields

$$C_2(t) = 1 - \frac{x_f^2}{2}\dot{h}_f \quad (C_2 > 0).$$

Here, $\tilde{w}(x_f,t) = -1$, since $x = x_f$ lies at the right endpoint of the top facet and away from the maximum. (Note that $w(h_x) = h_x/|h_x| = -1$ on the right of the facet, by Assumption A2.)

Hence, we obtain the system

$$\begin{cases} \displaystyle\int_0^{x_f} \ln\left(\frac{s^2}{2}\dot{h}_f + 1 - \frac{x_f^2}{2}\dot{h}_f \right) \mathrm{d}s = 1, \\ \dot{x}_f(h_0(x_f) - h_f) = \dot{h}_f x_f. \end{cases} \tag{25}$$

The first equation reads

$$\int_0^{x_f\sqrt{\frac{|\dot{h}_f|}{2}}} \ln\left(1 - \frac{x_f^2}{2}\dot{h}_f - \xi^2 \right) \mathrm{d}\xi = \sqrt{\frac{|\dot{h}_f|}{2}}.$$

This equation is simplified by use of the integral

$$\int_0^a \ln\left(1 + a^2 - \xi^2\right) \mathrm{d}\xi = -2a + 2i\sqrt{1+a^2}\tan^{-1}\left(-i\frac{a}{\sqrt{1+a^2}} \right).$$

Recall that the (in principle multivalued) function $\tan^{-1} z$ is expressed as

$$\tan^{-1} z = \frac{1}{2i}\ln\left(\frac{1+iz}{1-iz} \right).$$

Accordingly, the above integral is written as

$$\int_0^a \ln\left(1 + a^2 - \xi^2\right) \mathrm{d}\xi = -2a + \sqrt{1+a^2}\ln\left(\frac{\sqrt{1+a^2}+a}{\sqrt{1+a^2}-a} \right),$$

where the logarithm takes real values here. By use of the definition

$$X_f = x_f\sqrt{\frac{|\dot h_f|}{2}}, \tag{26}$$

we find that (25) can be written as

$$\begin{cases} 2\sqrt{1+X_f^2}\,\ln\left(X_f+\sqrt{1+X_f^2}\right)-2X_f=\sqrt{\dfrac{|\dot h_f|}{2}}, \\ \dot x_f(h_0(x_f)-h_f)=\dot h_f x_f. \end{cases} \tag{27}$$

Eqs. (26) and (27) form a closed ODE system describing the top-facet dynamics. Because $\dot h_f < 0$, we may frame (26) and (27) as a system of differential–algebraic equations (DAE). These equations are now recast into a form that can be solved by implicit ODE solvers, viz.,

$$\begin{cases} \dot X_f = \frac{\dot x_f F(X_f)}{1-x_f F'(X_f)}, \\ \dot h_f = -2F(X_f)^2, \\ \dot x_f(h_0(x_f)-h_f) = -2x_f F(X_f)^2, \end{cases} \tag{28}$$

where

$$F(X_f) = 2\sqrt{1+X_f^2}\,\ln(X_f+\sqrt{1+X_f^2})-2X_f.$$

It is of interest to note that the algebraic equation for X_f suggests that the correct value for $X_f(0)$ is given by a solution of

$$x_f(0)\left[2\sqrt{1+X_f^2}\,\ln\left(X_f+\sqrt{1+X_f^2}\right)-2X_f\right]-X_f=0, \tag{29}$$

which has three roots given by $X_f = 0,\ \pm g(x_f)$. The nonzero roots $\pm g(x_f)$ for large X_f should take the form

$$g(x_f)\approx\frac{e^{\frac{1}{2x_f(0)}+1}}{2}.$$

We reach the conclusion that, under the dynamics of (28), there is *no restriction* on the initial width, $2x_f(0)$, of the facet for the expansion of the facet at later times, $t > 0$.

3.3. Dynamics of bottom facet

Let us now discuss the case where the facet possibly corresponds to a degenerate local minimum of the height profile. In this case, $\dot h_f > 0$ by Assumption A3. The dynamics in (25) are replaced by the system

$$\begin{cases} \displaystyle\int_0^{x_f}\ln\left(\frac{s^2}{2}\dot h_f+1-\frac{x_f^2}{2}\dot h_f\right)\mathrm{d}s=-1, \\ \dot x_f(h_0(x_f)-h_f)=\dot h_f x_f. \end{cases} \tag{30}$$

The first equation implies that $\frac{x_f^2}{2\dot h_f}\le 1$.

Accordingly, by changing variables we observe that

$$\int_0^{X_f}\ln\left(\xi^2+1-X_f^2\right)\mathrm{d}\xi=-\sqrt{\frac{\dot h_f}{2}}\le 0. \tag{31}$$

By integrating directly in view of $\dot h_f > 0$, we obtain the system

$$2\sqrt{1-X_f^2}\left[\tan^{-1}\left(\frac{\sqrt{1-X_f^2}}{X_f}\right)-\frac{\pi}{2}\right]+2X_f=\sqrt{\frac{\dot h_f}{2}},$$
$$\dot x_f(h_0(x_f)-h_f)=\dot h_f x_f.$$

The first equation can be written as

$$y\left(\tan^{-1}y-\frac{\pi}{2}\right)+1=\frac{1}{2x_f} \tag{32}$$

where

$$y=\frac{\sqrt{1-X_f^2}}{X_f}.$$

The left-hand side of (32) is bounded by 1 for $y \ge 0$ (in fact, it is monotonically decreasing from 1); while, if x_f is sufficiently small, the right-hand side gets arbitrarily large. Hence, we reach the conclusion that: *only if* $x_f(0) > \frac{1}{2}$ *is it possible to find a solution with a moving bottom facet.*

As a result, facet solutions at minima are in fact fixed points of the evolution unless there is already a sufficiently long facet. This asymmetry in convexity and concavity of the morphological crystal surface evolution is consistent with observations of solutions to the exponential PDE in [8].

Remark 1. For the dynamics given by (6) as a nonlinear (weighted) H^{-1} gradient flow for the respective $E[h]$, the evolutions of top and bottom facets are distinctly different, precisely because of the effect of the exponential mobility, $e^{-\partial_x(\partial_x h/|\partial_x h|)}$. In particular, we predict that bottom facets have extremely slow (or non-existent) motion by diffusion, while top facets move relatively fast.

4. Numerical results

In this section, we present numerical results for the evolution of the height profile under sinusoidal initial data in 1+1 dimensions. We carry out numerics based on: (i) the ODE system discussed in Section 3; and (ii) the numerical solution of PDE (5) via the regularization of free energy (1). Specifically, we use the regularized surface free energy

$$E[h;\nu]=\int\left[\sqrt{|\nabla h|^2+\nu^2}+\frac{g}{3}|\nabla h|^3\right]\mathrm{d}x, \tag{33}$$

which has the regularization parameter $\nu > 0$.

4.1. Numerical approximation with $g = 0$

Next, we focus on the regularized versions of PDEs (21) and (23). The corresponding PDEs now read

$$\partial_t h=\partial_{xx}\exp\left\{-\partial_x\left(\frac{\partial_x h}{\sqrt{(\partial_x h)^2+\nu^2}}\right)\right\} \tag{34}$$

and

$$\partial_t h=-\partial_{xx}\partial_x\left(\frac{\partial_x h}{\sqrt{(\partial_x h)^2+\nu^2}}\right). \tag{35}$$

For discretizing both (34) and (35), we use the method of lines by applying a standard central finite difference discretization in space. The time integration of the resulting ODEs is then carried out with a fully implicit stepping scheme in time (by using routine ode15s in MATLAB).

Snapshots of solutions to evolution equations (34) and (35) under an initial height profile $h(0,x) = \sin x$ with $N = 60$ uniform grid points on the interval $[0, 2\pi]$ and $\nu = 10^{-3}$ by use of periodic boundary conditions can be seen in Fig. 2. We have chosen time scales such that the facets are evident in the numerical solutions. Note that exponential PDE (34) results in a strong asymmetry between regions of convexity and concavity, seen in the bottom left panel of Fig. 2. For each simulation, we have chosen the regularization parameter and the grid spacing such that the resulting derivatives are sufficient not only to allow facet motion but also to maintain a sharp facet boundary. In contrast to the clear convex/concave asymmetry of the numerical solution to

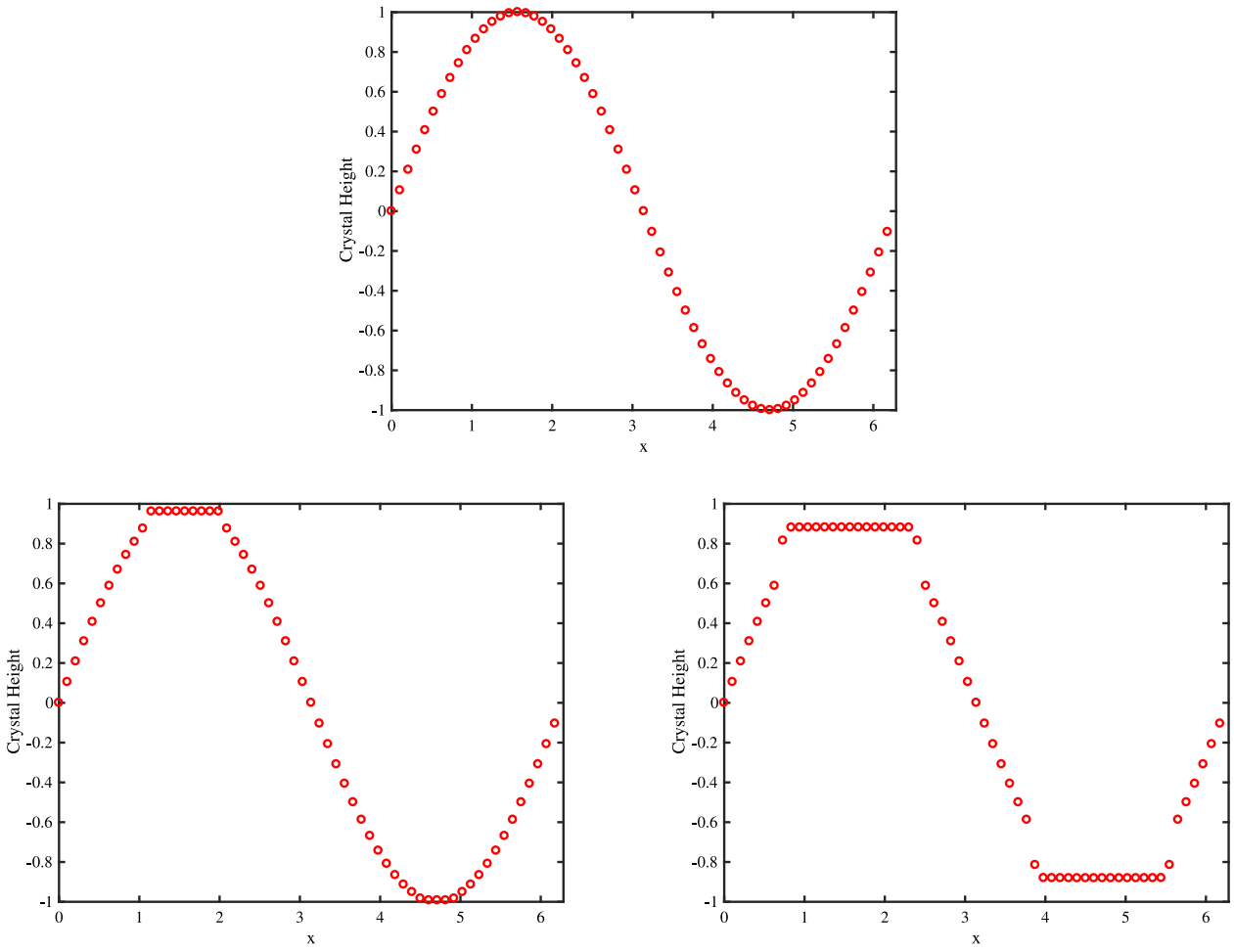

Fig. 2. Snapshots of evolving surface height profile, $h(x, t)$, under initial data $h(x, 0) = \sin(x)$ (top panel) by fourth-order total variation flows given by: exponential PDE (34) with regularization parameter $\nu = 10^{-3}$ on a time scale $T = 10^{-4}$ (bottom left panel); and by PDE (35) with regularization parameter $\nu = 10^{-3}$ on a time scale $T = 10^{-2}$ (bottom right panel).

(34), notice the symmetry in the solution of (35) in the bottom right panel of Fig. 2.

To verify that our numerical scheme is consistent, that is, the increase of resolution (number of grid points) improves or does not spoil the result, we plot a snapshot of the solution to (34) at time $T = 10^{-4}$ with $N = 60$ and $N = 120$ grid points; see Fig. 3. Notice that the numerical solution is stabilized, remaining practically unchanged with increasing N.

In Fig. 4, the evolution of PDE (34) is compared to ODE system (28) on time scales such that the facets are evident. In these simulations, the parameters for the PDE simulation are the same as above. To solve DAEs (28), we use the implicit ODE solver ode15i in MATLAB with explicitly chosen initial data for $X_f(0)$ as a non-zero root of (29). To generate the initial data $(x_f(0), h_f(0))$, we find it ideal to numerically solve PDE (34) for a short time ($\approx 5 \times 10^{-7}$). Then, we generate a non-singular (i.e. with $x_f(0) > 0$) initial configuration for the ODEs by reading off the maximum height of the resulting numerical facet solution and the outer extent of the facet position. Note that there is some sensitivity in how the initial data $x_f(0)$ is chosen given the discretization, which explains the small discrepancy observed in those plots involving $x_f(t)$. To compare the relevant parameters to the PDE evolution, we take

$$h_{f,pde}(t) = \max_{x\in[0,2\pi]} h(x, t),$$

$$x_f = \max\{x \in [0, 2\pi] : (\max_{x\in[0,2\pi]} h(x, t)) - h(x, t) < \varepsilon\}, \quad (36)$$

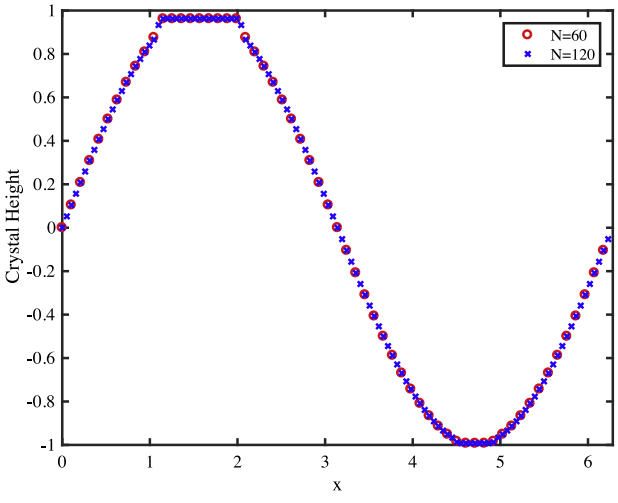

Fig. 3. (Color Online) Snapshots of evolving surface height profile, $h(x, t)$, for two different values ($N = 60,\ 120$) of the number, N, of grid points on a time scale $T = 10^{-4}$. The height $h(x, t)$ evolves according to exponential PDE (34) with initial data $h(x, 0) = \sin(x)$ and regularization parameter $\nu = 10^{-3}$.

where we typically choose $\varepsilon = 10^{-2}$. The data points for $x_f(t)$ in Fig. 4 appear to occur on larger time scales than the discretization

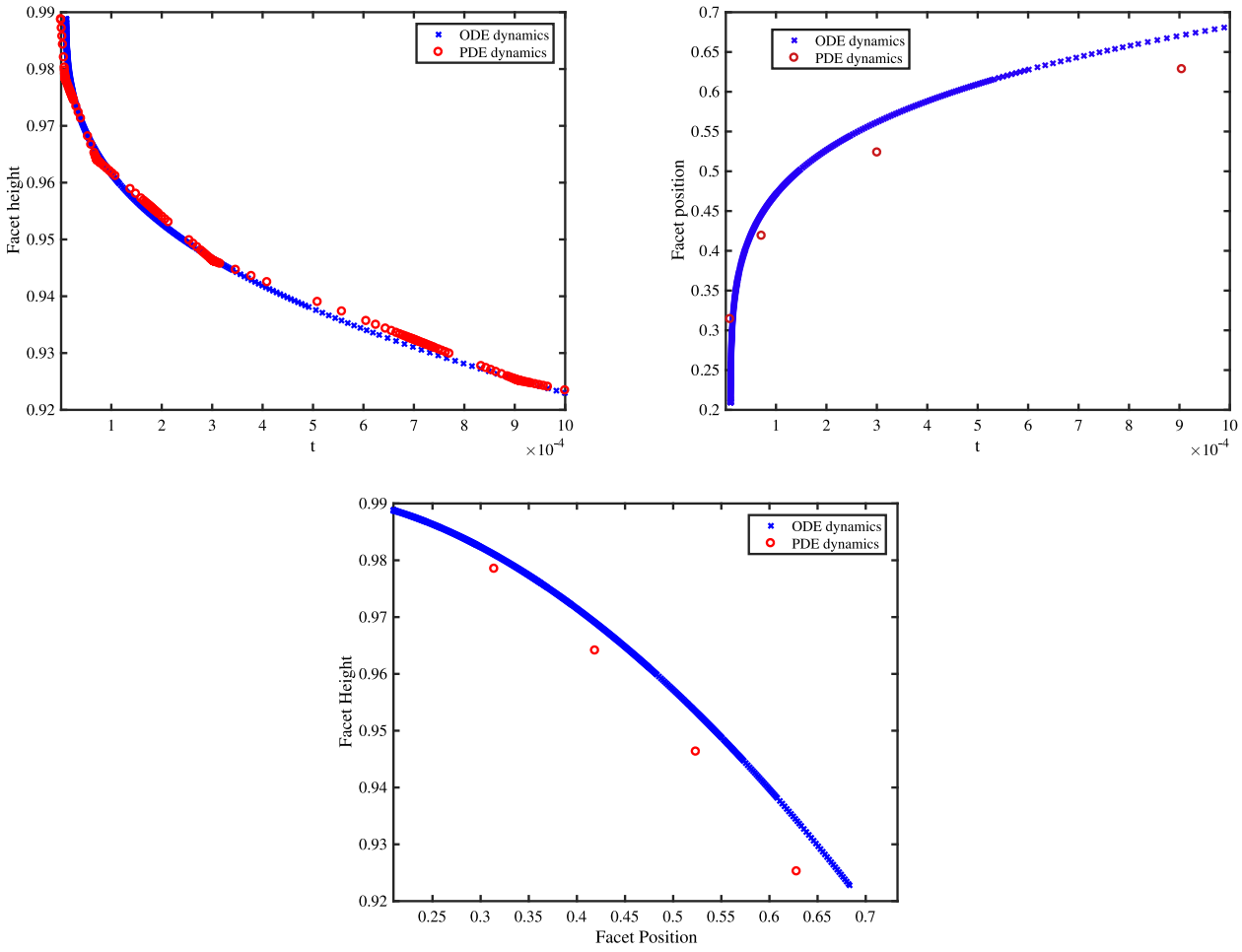

Fig. 4. (Color Online) Plots of facet height $h_f(t)$ versus time, t (top left panel), facet position $x_f(t)$ versus t (top right panel) and facet height versus facet position $(x_f(t), h_f(t))$ (bottom panel) for exponential PDE (34). In each plot, (x_f, h_f) as a solution of (28) is plotted using crosses (×); and the corresponding components of a solution to (34) as described in (36) are plotted using circles (○). The initial data for (28) is taken from the PDE evolution as $x_f(t_0) = \frac{\pi}{15}$, $h_f(t_0) = .98879899$ with $t_0 = 5 \times 10^{-7}$. The numerical experiments for the ODEs and PDE are then compared up to time $T = 10^{-3}$.

would suggest. However, this is purely a manifestation of the time required for the facet edge to travel from one discrete grid point to another in the numerical experiment. To make the figure clearer, we have thus only plotted times at which the solution has moved to a new grid point; the large gaps in data points for x_f are due entirely to the spatial grid size.

In Fig. 5, we carry out a similar numerical study as in Fig. 4, but now for the (non-weighted) H^{-1} total variation flow (35) studied, e.g., in [22,25–27]. The PDE evolution is compared to the ODE system (22) on time scales such that the (top and bottom) facets are evident. In these simulations, the discretizations for the PDE are the same as those used for the exponential PDE in this section.

4.2. Numerical approximation with $g > 0$

In this subsection, we focus on the case with nonzero step–step interactions ($g > 0$); see (1) and (33). Accordingly, we consider the fourth-order PDE

$$\partial_t h = \partial_{xx} e^{-\partial_x\left(\frac{\partial_x h}{|\partial_x h|} + g\partial_x h|\partial_x h|\right)}, \quad g > 0. \tag{37}$$

In this setting, we still observe asymmetry in the solution. However, due to presence of the (less singular) term $|\partial_x h|^3$ in the surface energy, the solution to this PDE no longer develops jumps in the height profile. This is expected from other studies in the (non-weighted) H^{-1} total variation flow; see e.g. [18]. Similarly to the case where $g = 0$, we can study the evolution numerically by using the regularized PDE

$$\partial_t h = \partial_{xx} e^{-\partial_x\left(\frac{\partial_x h}{\sqrt{(\partial_x h)^2+\nu^2}} + g\partial_x h|\partial_x h|\right)}, \tag{38}$$

which corresponds to the free energy functional $E[h; \nu]$ of (33).

In this case, there is no explicit ODE system to predict the dynamics of facets, since the underlying, regularized energy (33) does not permit the formation of jumps in height and facets (flat parts of the height profile) for $\nu, g > 0$. Indeed, our numerical scheme does not result in jumps in the height profile in this case, though of course the asymmetry of the exponential model is still manifest in the evolution; see Fig. 6 for a typical evolution of (37) with $g = 3$. For sufficiently small regularization parameter, ν, the numerical solution for h evolves to become quite flat near a maximum. This flat part of the height profile is still considered as a facet. In contrast, the height profile near a minimum seems to develop a discontinuity in the slope (see Fig. 6).

We note that the case with $g > 0$ in (37) results in dynamics similar to those observed in [8] with interaction potentials $V(z) = |z|^p$, $p > 1$. These dynamics include a flattening of the surface profile near the maximum of the initial height, and the finite-time formation of a discontinuity in the derivative of the height at the minimum of the initial height profile. We conjecture that these features are indeed expected in these types of degenerate fourth-order PDEs with exponential mobility. The reader is referred to [8]

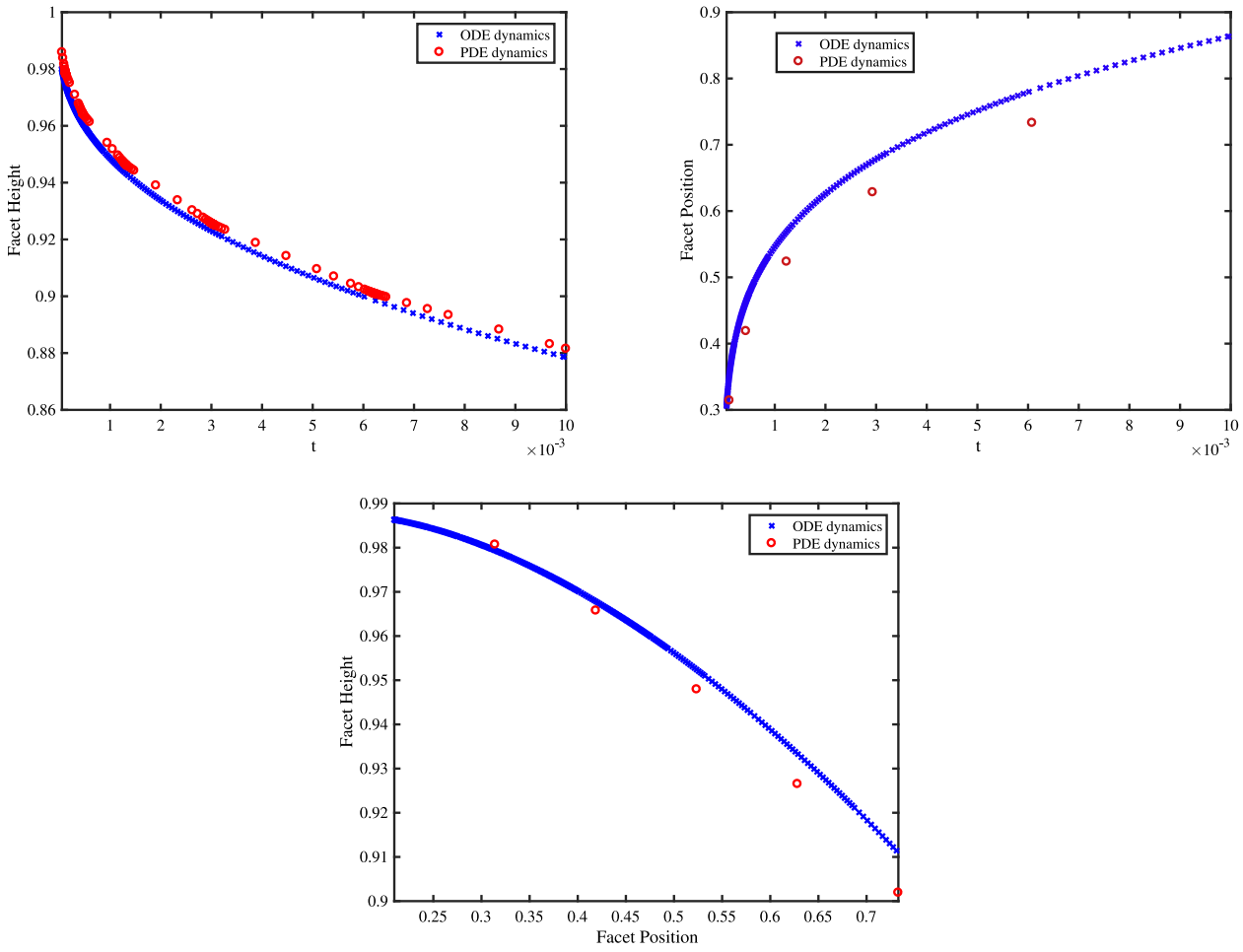

Fig. 5. (Color Online) Plots of facet height $h_f(t)$ versus time, t (top left panel), facet position $x_f(t)$ versus t (top right panel) and facet height versus facet position $(x_f(t), h_f(t))$ (bottom panel) for PDE (35). In each plot, (x_f, h_f) as a solution of (22) is plotted using crosses $(\times)$; and the corresponding components of a solution to (35) as described in (36) are plotted using circles $(\circ)$. The initial data for (22) is taken from the PDE evolution as $x_f(t_0) = \frac{\pi}{15}$, $h_f(t_0) = .98632751$ with $t_0 = 5 \times 10^{-5}$. The numerical experiments for the ODEs and PDE are then compared up to time $T = 10^{-2}$.

for a more detailed discussion of this type of breakdown of regularity in $\partial_x h$ in various settings.

5. Conclusion and discussion

In this paper, we studied plausible implications of continuum evolution law (5) which emerges from a mesoscale model for line defects and an atomistic broken-bond model in crystal surface morphological evolution. A noteworthy feature of this PDE is the presence of an exponential, singular mobility which has a significant effect if the Boltzmann energy, $k_B T$, is small compared to the step line tension. Because of this feature, the surface height evolution occurs in the framework of a nonlinear, weighted H^{-1} gradient flow for the convex free energy functional $E[h]$ of (1). For this evolution, in the absence of elasticity ($g = 0$), when evolution occurs by (6), we constructed a solution for the surface height in 1+1 dimensions that explicitly manifested an asymmetry between the dynamics on convex and concave parts of the crystal surface. This asymmetry manifests in the following way. Top facets expand fast, regardless of their initial size; in contrast, bottom facets move only if their size exceeds a certain critical length (see Remark 1).

Our analysis points to several open questions. For example, it is compelling to ask if the predicted facet asymmetry can be observed in one-dimensional periodic gratings in homoepitaxy. So far, we have focused on crystal surfaces in 1+1 dimensions. However, continuum evolution laws with an exponential mobility in 2+1 dimensions have been derived [8]; in addition, such PDEs are plausibly linked to step flow [6]. Therefore, the analysis of the dynamics stemming from such equations in higher dimensions is an interesting topic for future study. A related, pending issue is to understand the effects of (short- or long-range) elasticity on the facet evolution. In this case, the analytical description of facet dynamics is more challenging.

We note that the (non-weighted) H^{-1}-total variation flow (7) and the corresponding L^2-total variation flow have been studied in some detail by many authors, e.g. [22,25–27]. In the setting of the (weighted) H^{-1}-gradient flow with an exponential mobility, these studies fall into the more general framework of evolution equations of the form

$$h_t = \mathcal{L} e^{\mu[h]}, \quad h(x, 0) = h_0,$$

where $\mathcal{L}$ is an appropriate second-order differential operator dictated by the dominant kinetic processes in surface diffusion, e.g., $\mathcal{L} = \Delta$ for diffusion-limited kinetics; recall that the step chemical potential, $\mu[h]$, is the variation of the surface free energy. The analysis of evolutions of this form is still under development, including ODE dynamics for facets, existence of solutions in the total variation norm, and finite relaxation times (otherwise known as extinction times) to reach the equilibrium state in surface morphological relaxation. Similar issues arise in the theory of evolution PDEs of weighted L^2-total variation flow. These studies may shed light on the dynamics of various phenomena on crystal surfaces, e.g., the dewetting of thin, solid films [4].

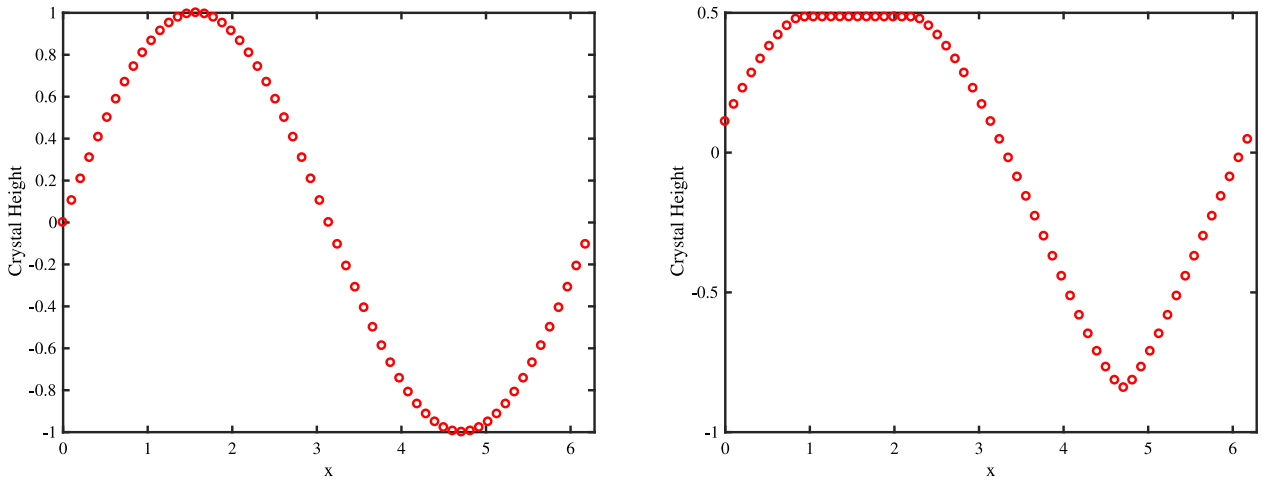

Fig. 6. Snapshots of surface height evolution by fourth-order, regularized flow (38). Left panel: Initial data $h_0(x) = \sin(x)$. Right panel: Height profile, $h(x, t)$, at $t = T = 10^{-1}$ with $\nu = 10^{-3}$ and $g = 3$.

It is worthwhile noting that the exponential PDE derived from atomistic dynamics in [8] with $p = 2$ has the form (for $\mathcal{L} = \Delta$)

$$\partial_t h = \Delta e^{-\Delta h}.$$

This PDE is studied in [49], where the authors derive weak solutions for a class of functions where Δh lives in a measure space. Extending such derivations and global dynamics to a general family of 4th-order degenerate PDE models with exponential mobility deserves attention for future research.

In the present work, we refrained from comparing the facet dynamics predicted by the continuum theory to the underlying microscale dynamics, particularly the motion of steps. An interesting feature in this context is the interaction between steps in the vicinity of a facet. This topic will be the subject of future work.

In a related fashion, the numerical schemes that we use here are based on straightforward finite-difference discretizations. Of course, energetic methods such as those for related problems in [18] motivated by algorithms developed in [50] would seem viable. However, the presence of the exponential mobility renders these methods much more computationally expensive. The convergence analysis and development of efficient numerical schemes for evolution equations of form (5) will be valuable for predictions of faceting in crystal surface morphological evolution.

Acknowledgments

The authors wish to thank Professors T.L. Einstein, Y. Giga, R.V. Kohn and J.Q. Weare for valuable discussions. The authors are also grateful to an anonymous reviewer for detailed and constructive comments on the manuscript, which contributed to its improvement. JGL was supported in part by the National Science Foundation (NSF), USA under award DMS-1812573. JL was supported in part by NSF, USA under award DMS-1454939. The research of the DM was supported by NSF DMS-1412769 at the University of Maryland, USA. The research of JLM was supported by NSF, USA Grant DMS-1312874 and NSF, USA CAREER Grant DMS-1352353. This collaboration was made possible thanks to the NSF, USA grant RNMS-1107444 (KI-Net).

Appendix. On the weighted H^{-1}-gradient flow

Following [25], we provide a formal discussion on the weighted H^{-1}-gradient flow for the PDE

$$h_t = \Delta e^{-\nabla\cdot\left(\frac{\nabla h}{|\nabla h|}\right)}, \tag{A.1}$$

which is formulated in the framework of weighted-H^{-1} subdifferential equation $h_t \in -\partial E(h)$ for an appropriately defined energy functional $E(h)$. For convenience, we take the spatial domain to be the torus, denoted $\mathbb{T}$ below.

A.1. Definition of weighted H^{-1}-subdifferential

Let X be a Banach space of functions whose derivatives are defined in some sense. For $h \in X$, consider a nonlinear mobility $M(h, \nabla h, \ldots)$ that is strictly positive. We choose not to specify the space X here. For example, X can be taken to be the space $W^{2,\infty}$. It is possible to justify the constructed solution in this space, since we can always add some regularity to the related scheme. Details for this topic lie outside the scope of this appendix; thus, we refrain from discussing them here. We use the nonlinear mobility M to define a local weighted Hilbert space $\mathcal{H}^1_h(\mathbb{T})$ as the completion of $C^\infty(\mathbb{T})$ with mean zero, under the weighted norm or inner product

$$\|v\|^2_{\mathcal{H}^1_h} = \int_{\mathbb{T}} M(h, \nabla h, \ldots)|\nabla v|^2 \,\mathrm{d}x, \tag{A.2}$$

$$(u, v)_1 = \int_{\mathbb{T}} M(h, \nabla h, \ldots)\nabla u(x)\cdot\nabla v(x)\,\mathrm{d}x. \tag{A.3}$$

We then define $\left(\mathcal{H}^1_h\right)^*$ as the dual space of $\mathcal{H}^1_h$ and let $\langle\cdot,\cdot\rangle$ be the duality pair.

Next, we define the duality mapping $J : \mathcal{H}^1_h \to \left(\mathcal{H}^1_h\right)^*$, $v \mapsto J(v)$ by

$$\langle J(v), u\rangle = (v, u)_1, \quad \forall u \in \mathcal{H}^1_h.$$

In this vein, we denote the duality mapping as $J(v) = -\Delta_h v$. If $v \in \mathcal{H}^2(\mathbb{T})$, we can show that

$$u\Delta_h v = u\nabla\cdot(M(h, \nabla h, \ldots)\nabla v)$$

is integrable, and

$$\langle J(v), u\rangle = (v, u)_1 = -\int_{\mathbb{T}} u\Delta_h v\,\mathrm{d}x.$$

Hence, we call Δ_h the weighted Laplacian operator.

Let $\phi \in \left(\mathcal{H}^1_h\right)^*$. Since $\mathcal{H}^1_h$ with inner product $(\cdot,\cdot)_1$ as defined by (A.3) is a Hilbert space, by the Riesz-Fréchet representation theorem there exists unique $f_\phi \in \mathcal{H}^1_h$ satisfying $\langle\phi, u\rangle = (f_\phi, u)_1$ for every $u \in \mathcal{H}^1_h$. Let us thus define the inverse map $J^{-1} : \left(\mathcal{H}^1_h\right)^* \to \mathcal{H}^1_h$, $\phi \mapsto J^{-1}(\phi)$ as $J^{-1}(\phi) = f_\phi$. Indeed, for any $\phi, \psi \in \left(\mathcal{H}^1_h\right)^*$, we thus also have the well-defined inner product of $\left(\mathcal{H}^1_h\right)^*$ by

$(\phi, \psi)_{-1} := \langle \psi, J^{-1}(\phi) \rangle$.

One can verify that $\left(\mathcal{H}_h^1\right)^*$ with this inner product is a Hilbert space. Let Δ_h^{-1} be the inverse operator of Δ_h in $\mathbb{T}$ with mean zero. If $\psi \Delta_h^{-1} \phi$ is integrable, we have

$$\langle J^{-1}(\phi), \psi \rangle = -\int_{\mathbb{T}} \psi(\Delta_h^{-1}\phi)\, \mathrm{d}x, \quad \forall \psi \in \left(\mathcal{H}_h^1\right)^*,$$

and, thus, $J^{-1}(\phi) = -\Delta_h^{-1}\phi$.

Let $E : X \to \mathbb{R} \cup \{\infty\}$, $h \mapsto E(h)$ be a convex functional. For a fixed $h \in X$, we extend the functional E to H_h^1 and define the weighted H^{-1}-subdifferential of this extended functional E at u in $\mathcal{H}_h^1$ as

$$\partial E(u) = \left\{ \phi \in \left(\mathcal{H}_h^1\right)^*,\ E(v) \geq E(u) + \langle \phi, v - u \rangle,\ \forall v \in \mathcal{H}_h^1 \right\}.$$

One can directly verify that $J(v) \in \partial E(v)$ for $E(v) = \frac{1}{2}\|v\|^2_{\mathcal{H}_h^1}$.

A.2. Example of total variation energy and curvature-dependent exponential mobility

The gradient flow of linear growth functionals $E(h)$ has been well studied; see, e.g., [51]. Here, we use the total variation energy $E(h) = \int_{\mathbb{T}} |\nabla h|\, \mathrm{d}x$ defined as

$$E(h) = \sup_{\varphi} \left\{ \int_{\mathbb{T}} \nabla h \cdot \varphi \, \mathrm{d}x \;\middle|\; \|\varphi\|_{L^\infty(\mathbb{T})} \leq 1, \varphi \in L^\infty(\mathbb{T}) \right\}.$$

Consider the level set mean curvature-dependent exponential mobility

$$M(h, \nabla h, \ldots) = e^{-\nabla \cdot \left(\frac{\nabla h}{|\nabla h|}\right)}.$$

Next, we will find $\phi \in \left(\mathcal{H}_h^1\right)^*$ such that (see Appendix A.1 of this appendix)

$$\frac{E(h + \varepsilon v) - E(h)}{\varepsilon} = \langle \phi, v \rangle + o(1) \quad \text{as } \varepsilon \to 0. \tag{A.4}$$

The left-hand side of the above expression is written as

$$\frac{E(h + \varepsilon v) - E(h)}{\varepsilon} = \int_{\mathbb{T}} \frac{|\nabla(h + \varepsilon v)| - |\nabla h|}{\varepsilon}\, \mathrm{d}x$$
$$= \int_{\mathbb{T}} \frac{\nabla h}{|\nabla h|} \cdot \nabla v \, \mathrm{d}x + o(1) = -\int_{\mathbb{T}} v\, \nabla \cdot \left(\frac{\nabla h}{|\nabla h|}\right) \mathrm{d}x + o(1)$$
$$= -\int_{\mathbb{T}} v (\Delta_h)^{-1} \Delta_h \nabla \cdot \left(\frac{\nabla h}{|\nabla h|}\right) \mathrm{d}x + o(1), \ \text{as } \varepsilon \to 0.$$

Let

$$\phi = \Delta_h \nabla \cdot \left(\frac{\nabla h}{|\nabla h|}\right) = -\Delta\, e^{-\nabla \cdot \left(\frac{\nabla h}{|\nabla h|}\right)}.$$

Hence, we obtain (A.4). By use of this formulation, (A.1) can thus be recast to the form $h_t = -\phi$, which we regard as the weighted $H^{-1}(\mathbb{T})$-gradient flow for energy functional $E(h)$.

A.3. Semi-implicit Euler scheme approximation

In this subsection, we informally discuss a semi-implicit Euler scheme for PDE (A.1). For a general discussion on the minimizing movement approach to gradient flow dynamics, see, e.g., [52]. To indicate the appropriate interpretation for the gradient flow that we study here, let us now discretize in time so that $h^n := h(x, n\tau)$, where τ is the time step. For a given $h^{n-1} \in BV(\mathbb{T})$, define

$$\Phi(h; h^{n-1}, \tau) := E(h) + \frac{1}{2\tau}\|h - h^{n-1}\|^2_{\mathcal{H}^{-1}_{h^{n-1}}},$$

where

$$\|h - h^{n-1}\|^2_{\mathcal{H}^{-1}_{h^{n-1}}} = -\int (h - h^{n-1}) \Delta^{-1}_{h^{n-1}} (h - h^{n-1})\, \mathrm{d}x.$$

We discretize in time by using the unconditionally-stable semi-implicit Euler scheme [52], viz.,

$$h^n \in \operatorname{argmin} \Phi(\cdot; h^{n-1}, \tau).$$

By convexity, there is a unique $h^n \in BV(\mathbb{T})$ satisfying

$$\frac{h^n - h^{n-1}}{\tau} = \Delta_{h^{n-1}} \nabla \cdot \left(\frac{\nabla h^n}{|\nabla h^n|}\right)$$
$$= \nabla \cdot \left(e^{-\nabla \cdot \left(\frac{\nabla h^{n-1}}{|\nabla h^{n-1}|}\right)} \nabla \nabla \cdot \left(\frac{\nabla h^n}{|\nabla h^n|}\right)\right)$$

with

$$E(h^n) + \frac{1}{2\tau}\|h^n - h^{n-1}\|^2_{\mathcal{H}^{-1}_{h^{n-1}}} \leq E(h^{n-1}).$$

We thus define

$$h^\tau(x, t) = h^n, \quad \text{if } t \in [n\tau, (n+1)\tau),$$

and, as $\tau \to 0$, $h^\tau(x, t)$ approaches a solution of (A.1).

References

[1] A. Pimpinelli, J. Villain, Physics of Crystal Growth, Cambridge University Press, Cambridge, UK, 1999.
[2] H.-C. Jeong, E.D. Williams, Steps on surfaces: experiment and theory, Surf. Sci. Rep. 34 (1999) 171–294.
[3] C. Misbah, O. Pierre-Louis, Y. Saito, Crystal surfaces in and out of equilibrium: a modern view, Rev. Modern Phys. 82 (2010) 981–1040.
[4] A. Chame, O. Pierre-Louis, Modeling dewetting of ultra-thin solid films, C. R. Phys. 14 (2013) 553–563.
[5] W.K. Burton, N. Cabrera, F.C. Frank, The growth of crystals and the equilibrium structure of their surfaces, Philos. Trans. R. Soc. Lond. Ser. A 243 (1951) 299–358.
[6] D. Margetis, R.V. Kohn, Continuum relaxation of interacting steps on crystal surfaces in 2+1 dimensions, Multiscale Model. Simul. 5 (2006) 729–758.
[7] J. Krug, H.T. Dobbs, S. Majaniemi, Adatom mobility for the solid-on-solid model, Z. Phys. B 97 (1995) 281–291.
[8] J.L. Marzuola, J. Weare, The relaxation of a family of broken bond crystal surface models, Phys. Rev. E 88 (2013) 032403.
[9] J.S. Rowlinson, B. Widom, Molecular Theory of Capillarity, Clarendon Press, Oxford, 1982.
[10] B. Krishnamachari, J. McLean, B. Cooper, J. Sethna, Gibbs-Thomson formula for small island sizes: corrections for high vapor densities, Phys. Rev. B 54 (1996) 8899–8907.
[11] R.V. Kukta, K. Bhattacharya, A micromechanical model of surface steps, J. Mech. Phys. Solids 50 (2002) 615–649.
[12] R.V. Kukta, A. Peralta, D. Kouris, Elastic interaction of surface steps: effect of atomic-scale roughness, Phys. Rev. Lett. 88 (2002) 186102.
[13] V.B. Shenoy, A. Ramasubramaniam, H. Ramanarayan, D.T. Tambe, W.-L. Chan, E. Chason, Influence of step-edge barriers on the morphological relaxation of nanoscale ripples on crystal surfaces, Phys. Rev. Lett. 92 (2004) 256101.
[14] A. Bonito, R.H. Nochetto, J. Quah, D. Margetis, Self-organization of decaying surface corrugations: a numerical study, Phys. Rev. E 79 (2009) 050601(R).
[15] A. Zangwill, C.N. Luse, D.D. Vvedensky, M.R. Wilby, Epitaxial growth and recovery: an analytical approach, Mater. Res. Soc. Symp. Proc. 237 (1992) 189–198.
[16] S. Tanaka, C.C. Umbach, J.M. Blakely, Atomic step distributions on annealed periodic Si(001) gratings, J. Vac. Sci. Technol. A 15 (1997) 1345–1350.
[17] N. Israeli, D. Kandel, Decay of one-dimensional surface modulations, Phys. Rev. B 62 (2000) 13707–13717.
[18] R.V. Kohn, E. Versieux, Numerical analysis of a steepest-descent PDE model for surface relaxation below the roughening temperature, SIAM J. Num. Anal. 48 (2010) 1781–1800.
[19] M. Ozdemir, A. Zangwill, Morphological equilibration of a corrugated crystalline surface, Phys. Rev. B 42 (1990) 5013–5024.
[20] A. Rettori, J. Villain, Flattening of grooves on a crystal surface: a method of investigation of surface roughness, J. Phys. Fr. 49 (1988) 257–267.
[21] V.B. Shenoy, L.B. Freund, A continuum description of the energetics and evolution of stepped surfaces in strained nanostructures, J. Mech. Phys. Solids 50 (2002) 1817–1841.
[22] R. Kobayashi, Y. Giga, Equations with singular diffusivity, J. Stat. Phys. 95 (1999) 1187–1220.

[23] I.V. Odisharia, Simulation and analysis of the relaxation of a crystalline surface, Ph. D. Thesis, Courant Institute, New York University, 2006.
[24] H.P. Bonzel, E. Preuss, Morphology of periodic surface profiles below the roughening temperature: aspects of continuum theory, Surf. Sci. 336 (1995) 209–224.
[25] M.H. Giga, Y. Giga, Very singular diffusion equations: second and fourth order problems, Japan J. Indust. Appl. Math. 27 (2010) 323–345.
[26] Y. Giga, R.V. Kohn, Scale-invariant extinction time estimates for some singular diffusion equations, Discr. Cont. Dyn. Sys. A 30 (2011) 509–535.
[27] Y. Giga, H. Kuroda, H. Matsuoka, Fourth-order total variation flow with Dirichlet condition: characterization of evolution and extinction time estimates, Adv. Math. Sci. Appl. 24 (2014) 499–534.
[28] H. Al Hajj Shehadeh, R.V. Kohn, J. Weare, The evolution of a crystal surface: analysis of a one-dimensional step train connecting two facets in the ADL regime, Physica D 240 (2011) 1771–1784.
[29] N. Israeli, H.-C. Jeong, D. Kandel, J.D. Weeks, Dynamics and scaling of one-dimensional surface structures, Phys. Rev. B 61 (2000) 5698–5706.
[30] N. Israeli, D. Kandel, Profile of a decaying crystalline cone, Phys. Rev. B 60 (1999) 5946–5962.
[31] D. Margetis, P.-W. Fok, M.J. Aziz, H.A. Stone, Continuum theory of nanostructure decay via a microscale condition, Phys. Rev. Lett. 97 (2006) 096102.
[32] E.E. Gruber, W.W. Mullins, On the theory of anisotropy of crystalline surface tension, J. Phys. Chem. Solids 28 (1967) 875–887.
[33] R. Najafabadi, D.J. Srolovitz, Elastic step interactions on vicinal surfaces of fcc metals, Surface Sci. 317 (1994) 221–234.
[34] L.B. Freund, S. Suresh, Thin Film Materials: Stress, Defect Formation and Surface Evolution, Cambridge University Press, Cambridge, UK, 2009.
[35] H. Xu, Y. Xiang, Derivation of a continuum model for the long-range elastic interaction on stepped epitaxial surfaces in $2+1$ dimensions, SIAM J. Appl. Math. 69 (2009) 1393–1414.
[36] A. Zangwill, C.N. Luse, D.D. Vvedensky, M.R. Wilby, Equations of motion for epitaxial growth, Surf. Sci. Let. 274 (1991) 529–534.
[37] T. Ihle, C. Misbah, O. Pierre-Louis, Equilibrium step dynamics on vicinal surfaces revisited, Phys. Rev. B 58.4 (1998) 2289.
[38] J.D. Weeks, G.H. Gilmer, Dynamics of crystal growth, Adv. Chem. Phys. 40 (1979) 157–228.
[39] W.-L. Chan, A. Ramasubramaniam, V.B. Shenoy, E. Chason, Relaxation kinetics of nano-ripples on Cu(001) surface, Phys. Rev. B 70 (2004) 245403.
[40] H. Spohn, Surface dynamics below the roughening transition, J. Phys. I (France) 3 (1993) 69–81.
[41] Y. Kashima, A subdifferential formulation of fourth order singular diffusion equations, Adv. Math. Sci. Appl. 14 (2004) 49–74.
[42] I. Fonseca, G. Leoni, Y.Y. Lu, Regularity in time for weak solutions of a continuum model for epitaxial growth with elasticity on vicinal surfaces, Comm. Partial Differential Equations 40 (2015) 1942–1957.
[43] J. Lu, J.-G. Liu, D. Margetis, Emergence of step flow from an atomistic scheme of epitaxial growth in $1+1$ dimensions, Phys. Rev. E 91 (2015) 032403.
[44] D. Margetis, Unified continuum approach to crystal surface morphological relaxation, Phys. Rev. B 76 (2007) 193403.
[45] V.I. Marchenko, A. Ya. Parshin, Elastic properties of crystal surfaces, Soviet Phys. JETP 52 (1980) 129–131.
[46] T. Funaki, Stochastic Interface Models, Lectures on Probability Theory and Statistics, in: Lecture Notes in Mathematics 1869, Springer, Berlin, 2005, pp. 103–274.
[47] T. Funaki, H. Spohn, Motion by mean curvature for the Ginzburg-Landau $\nabla\phi$ interface model, Comm. Math. Phys. 185 (1997) 1–36.
[48] T. Nishikawa, Hydrodynamic limit for the Ginzburg-Landau $\nabla\phi$ interface model with a conservation law, J. Math. Sci. Univ. Tokyo 9 (2002) 481–519.
[49] J.-G. Liu, X. Xu, Existence theorems for a multidimensional crystal surface model, SIAM J. Math. Anal. 48 (2016) 3667–3687.
[50] R. Jordan, D. Kinderlehrer, F. Otto, The variational formulation of the Fokker–Planck equation, SIAM J. Math. Anal. 29 (1998) 1–17.
[51] F. Andreu-Vaillo, V. Caselles, J.M. Mazón, Parabolic quasilinear equations minimizing linear growth functionals, vol. 223, Springer Science & Business Media, 2004.
[52] L. Ambrosio, N. Gigli, G. Savaré, Gradient flows: in metric spaces and in the space of probability measures, Springer Science & Business Media, 2008.